Mineralogy And Petrology
August 2022, Volume 116 Issue 4 Pages 311-335
https://doi.org/10.1007/s00710-022-00786-y
https://archimer.ifremer.fr/doc/00865/97695/

Variscan lamprophyres of the South Armorican Domain and comparison with lamprophyres of the Western European Variscan belt

Pouclet André [1, *], Bardintzeff Jacques-Marie [2], Bellon Hervé [3]

[1] Institute of Earth Sciences, University of Orléans, 3, rue des foulques, 45000, 85560, Orléans, Longeville-sur-mer, France
[2] UMR CNRS 8148 GEOPS, University Paris-Saclay, Sciences de La Terre, bât. 504, 91405, Volcanologie, PlanétologieOrsay, France
[3] University of Brest Laboratoire Géosciences Océan, Institut Universitaire Européen de La Mer, Place Nicolas Copernic, 29280, Plouzané, France

* Corresponding author : André Pouclet, email address : andre.pouclet@sfr.fr

Abstract :

Late to post-orogenic lamprophyres of the European Variscides attest variable compositions of the mantle beneath the structural zones of the belt. These compositions resulted from different contributions of mantle components involving geotectonic processes during the orogeny, such as oceanic subduction of mafic crust and sediments, continental subduction, collision with mantle input, and delamination of overriding plates. For documenting these processes, we have surveyed three sites of lamprophyre intrusions in the Vendean part of the South Armorican tectonic Zone with spessartite sills and minette dykes, and a fourth site in the West-Armorican kersantite swarm. The age of spessartite is estimated between 320 and 315 Ma on the base of structural relationships with the dated neighbouring granite. Dykes of minette share similar intrusive setting along the post-orogenic NW-SE dextral shear zones. One dyke is dated at 286.2 +/- 6.6 Ma (Early Permian) by K/Ar method. The Western Brittany kersantite swarm is Middle to Late Carboniferous in age. All these rocks display common mineral and chemical compositions of lamprophyres. A review of the Variscan European lamprophyres is conducted in order to document their geochemical fingerprints compared with those of the studied samples.

Keywords : Lamprophyre, Variscan belt, South-Armorican zone, West-European Variscides, Late and post-orogenic magmatism

Introduction

Lamprophyre dykes and sills are common throughout the Western European Variscan realm from England and France to Germany, Czech Republic, Poland, and Spain (Fig. 1). The lamprophyric occurrences also extend north of the Variscan orogenic front in Scotland, Norway, and Sweden (Kirstein et al. 2006). The widespread dyke and sill swarms are dated from Late Devonian to Permian and can be devoted from syn- to post-orogenic magmatic activities of the Variscan belt. They display various calc-alkaline and alkaline to peralkaline compositions with spessartites, vogesites, kersantites, minettes, camptonites, and monchiquites, some being associated with lamproites. Arguably, such large compositional and age ranges betray different geodynamics and magmatic conditions of genesis.

Petrogenesis of lamprophyres was a long-standing matter of debate. Once it was admitted that lamprophyres may represent primary-mantle melts (Rock 1987, 1991), different sources and melting conditions were considered. Present statement rather favours a deep depth melting of metasomatized mantle sources previously enriched in large ion lithophile and high field strength elements, with the contribution of subducted continental crust and/or altered oceanic lithosphere. Enrichment may be found in subduction related processes from assimilation of the sedimentary cover or from mixing with fluids or melts resulting from partial melting of subducted material. Diversity of lamprophyre magmas resulted from various combinations of magma mixing and mingling, fractional crystallization,

---

1

2

3

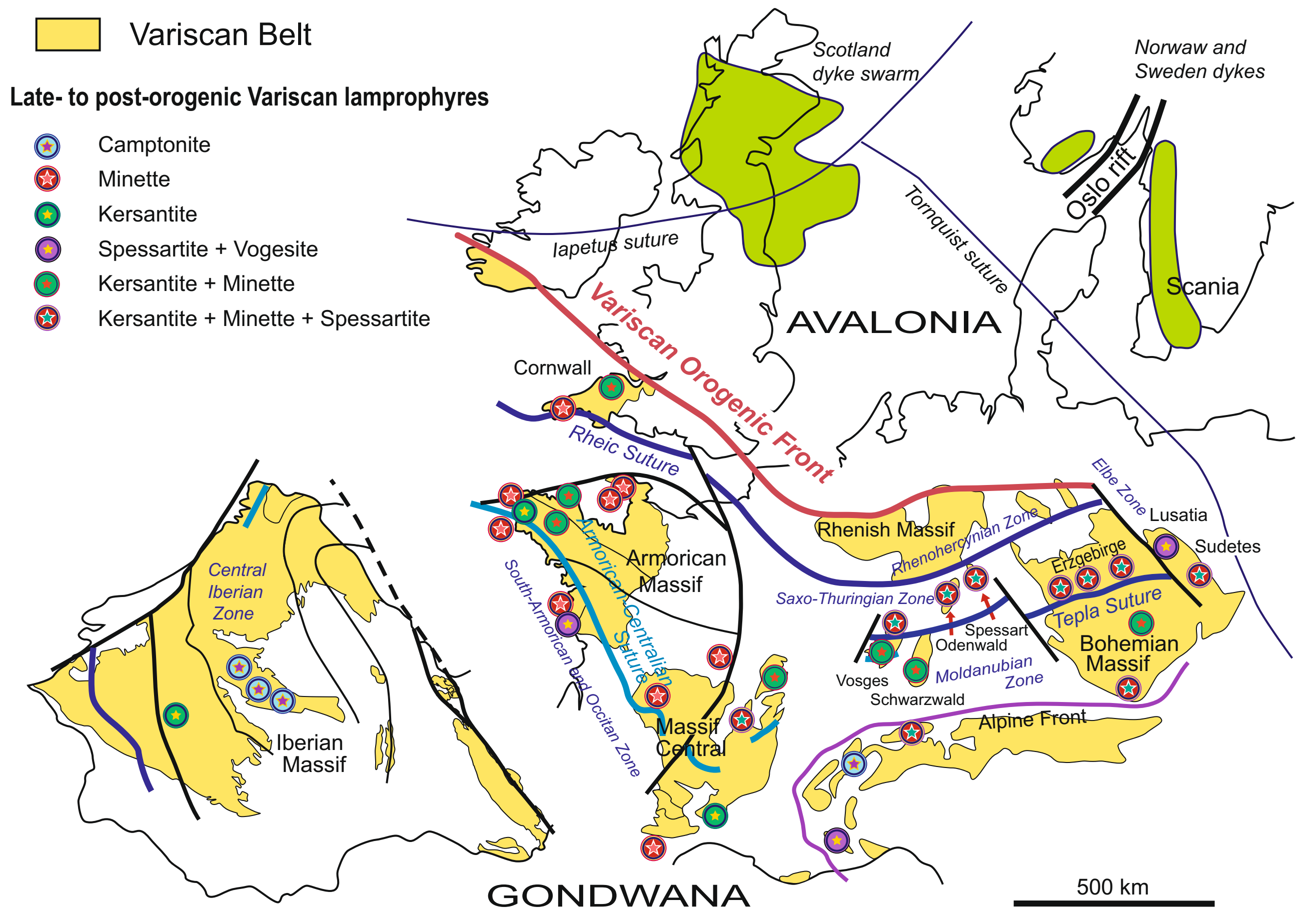

Fig. 1 Late to post-orogenic lamprophyres of the Variscan Belt. Map of the Variscan massifs at the Permian time after Ballèvre et al. (2009) and Pouclet et al. (2017). Northern Europe intrusions after Kirstein et al. (2006). Location of lamprophyre sites after references cited in this work

assimilation of crustal components and volatile enrichment (Turpin et al. 1988; Hegner et al. 1998; von Seckendorff et al. 2004; Awdankiewicz 2007; Seifert 2008; Soder and Romer 2018; Krmiček et al. 2020a, b).

In the South Armorican Domain, we investigated sills and dykes of spessartite and minette in the Vendean Atlantic coast and a sill of kersantite in the westernmost Brittany area, for their petrological and geochemical features. The aim of this work is to discuss the geotectonic and magmatic significances of this regional lamprophyric activity, taking into account recent and numerous accurate studies of the lamprophyres widely distributed in the whole European Variscan belt.

West Vendean lamprophyres: Geological background

Generalities

The West Vendean lamprophyres consist of sills and dykes intruding the Variscan structural Units along the Atlantic coast (Fig. 2). We distinguish two different lamprophyre types: amphibole-bearing spessartite and biotite-bearing minette. Thin sills of spessartite are located in the La Chaume sea cliff, west of the harbour of Les Sables-d'Olonne. Dykes of minette are located at two mains sites of the seashore: Croix-de-Vie, west of the harbour of Saint-Gilles-Croix-de-Vie, and Payré, west of the Payré rocky foreland and south-east of Les Sables-d'Olonne. Some dykes were pointed out on land, but are badly preserved.

La Chaume spessartite

Along the southern sea cliff of La Chaume, numerous lamprophyre sills are intruded in between orthogneiss layers (Figs. 3 and 4). The gneisses are dated to Early Cambrian and belong to the Complex of Les Sables-d'Olonne (Fig. 2) (Pouclet et al. 2017). The lamprophyres are not metamorphosed but are set in conformity with the metamorphic foliation trending W-E with a N 110° stretch lineation and a 30° dip to the north. Unless than twelve thin intrusions are distributed in a limited section of the cliff, about 160 m

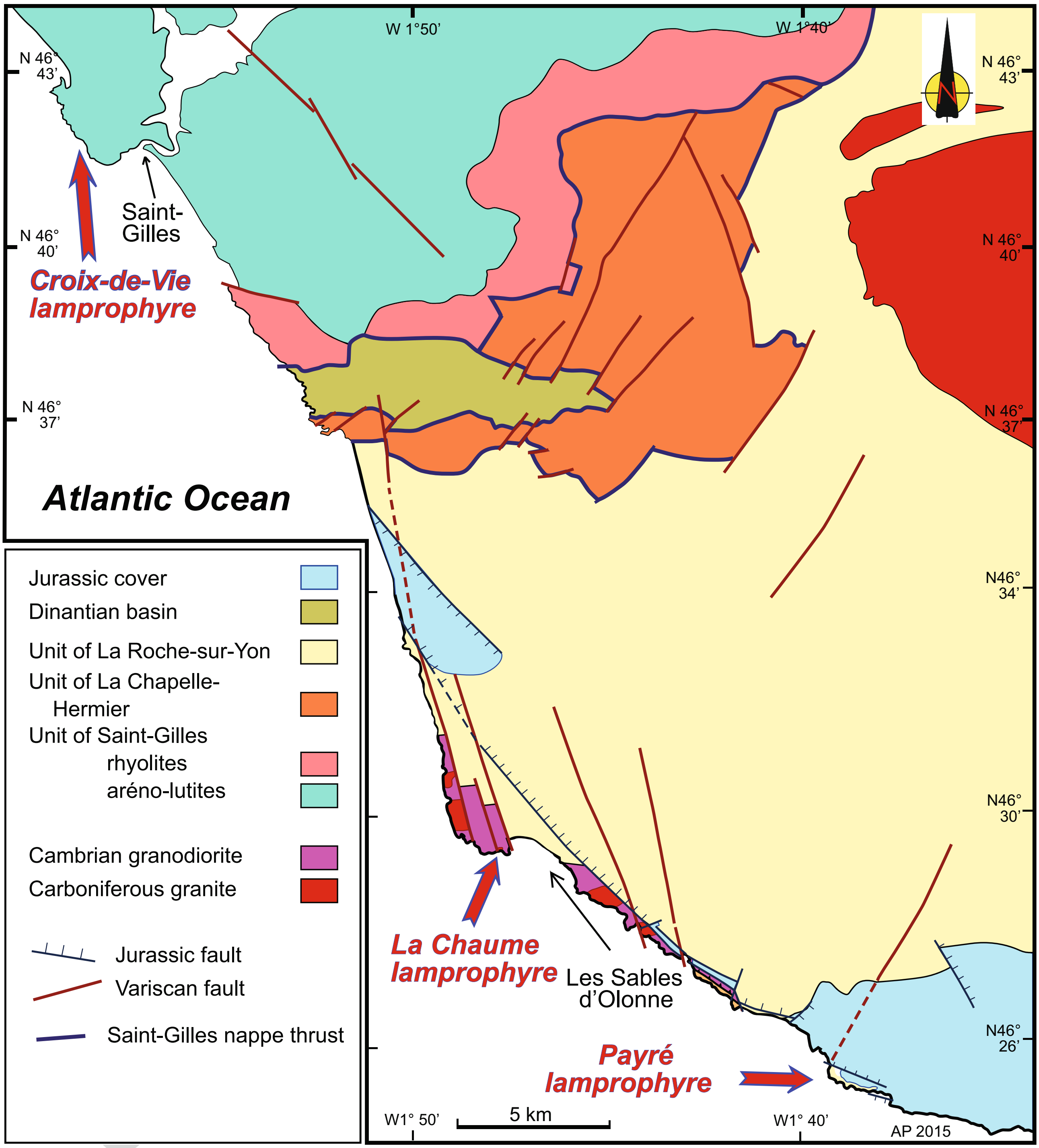

Fig. 2 Location of the Variscan lamprophyres in the Vendean part of the South-Armorican and Occitan Zone. Map after Pouclet (2016). The best outcrops are located on the sea shore in three main sites: Croix-de-Vie, La Chaume and Payré from north to south

from west to east and 20 m high. All these sills are similar and determined as spessartite. Their thickness ranges from 10 to 100 cm and their length from 30 to 80 m. They are located above a thick cupola of pegmatite inserted within the gneiss unit. The upper sill is the most extended to the west side where it gains the highest thickness of one metre. Some sills are bordered by layers of pegmatite, suggesting a sub-contemporary setting. The sill margins display a 2 cm-thick layer of biotite that can be explained by a vapour pressure effect of the gas-rich lamprophyric magma with

Journal : Large 710	Article No : 786	Pages : 25	MS Code : 786	Dispatch : 1-7-2022

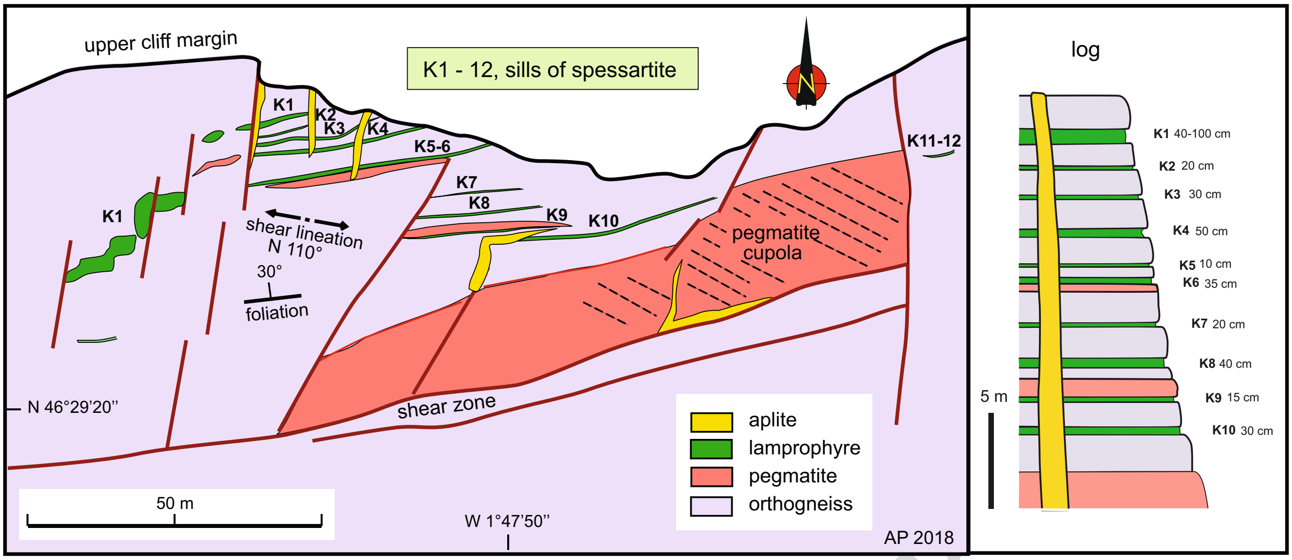

Fig. 3 La Chaume site of the sills of spessartite in a sketch of the cliff. Succession of the sills intruded in the gneiss foliation, as well as pegmatite bodies. Vertical scale and sill thicknesses are indicated in a log. The aplite dykes crosscut both lamprophyres and pegmatites

mica neo-crystallization. Some margins are also enriched in large and oriented crystals of microcline, muscovite and quartz from neighbouring pegmatite veins. The margins are stretched in W-E average trend but the inner part of the sills shows no textural orientation and is made of fine isometric grains. These features attest for the intrusion of the lamprophyre magma at the time of a pegmatitic event. This event can be related to the pneumatolytic stage of the underlying granite pluton of Les Sables-d'Olonne that outcrops northwest and east of La Chaume and is dated around 320 Ma (Turillot et al. 2011). Afterwards, the lamprophyre margins together with gneisses and pegmatites have registered the W-E regional tectonic shearing dated to the late early Carboniferous (Pouclet et al. 2017). Moreover, all the formations are crosscut by dykes of aplite, a few centimetres to 100 cm thick, associated with left-lateral vertical shear faults trending N 10°. There is clear evidence that the lamprophyre magma emplaced in the gneissic roof of the pluton at the time of the granite solidification.

Croix-de-Vie and Payré minettes

Dykes of lamprophyres intruded the cliff and the foreshore of Croix-de-Vie, west of the Saint-Gilles-Croix-de-Vie (Fig. 2). This area consists of low-grade metamorphic shales and sandstones of the Saint-Gilles Unit dated to Ordovician, trending WNW-ESE and dipping 20° to the north (Pouclet et al. 2017). We distinguish three intrusions in the cliff and three others in the shore (Fig. 5). (1) The first dyke crosscuts the cliff in trending N 30°, with vertical margins, and 2.9 m in width. The rock consists of a fine grained biotite-rich lamprophyre of regular size in the whole body. It is determined as a minette. (2) Close to the west side of this great dyke, a metre-thick intrusion of the same rock crosscuts the metasedimentary layers in one part and is inserted in the hinge line of the folds in another part like a chonolite body. (3) In a western buttress of the cliff, a third 10 to 20 cm thick intrusion extended to about 4 m from the base to the top of the cliff. This thin dyke was laterally supplied with the same fined grained minette. (4) To the west side of the sandy beach, a 4 to 5 m wide and N 45° trending vertical dyke crosscuts the rocky upper foreshore along 40 m. It approximately continues the great dyke of the cliff below the sandy beach but with a possible left-lateral shift, taking into account the location of a shear tectonic line at the foot of the cliff. This fourth dyke is sharply cut by a NW–SE left-lateral shear fault across the rocky shore. (5) This dyke is continued with a fifth dyke after a 65 m left-lateral motion along the shear fault. This new dyke is dipped to the north and bended to the southwest along a 40 m course. (6) A sixth dyke is a NE-SW-tending en echelon relay. This last dyke extends to the seaward and disappears in deep water after about 70 m of length.

In the Payré area, two lamprophyre dykes are en echelon relayed across the shore until to the cliff, with a N 80° average trend (Fig. 6). They crosscut the low grade metamorphic sandstones of the lower formation of La Roche-sur-Yon Unit that is N 125° trending and 65° dipping to the north-east, and dated to the early Ordovician. The dyke # 1 extends from the cliff to the foreshore and is 140 m of length with an average thickness of 1.8 m. The dyke # 2 extends from the middle shore to the seaward after a visible course of 80 m. Its average thickness is 80 cm. Both dykes are vertical to 60°

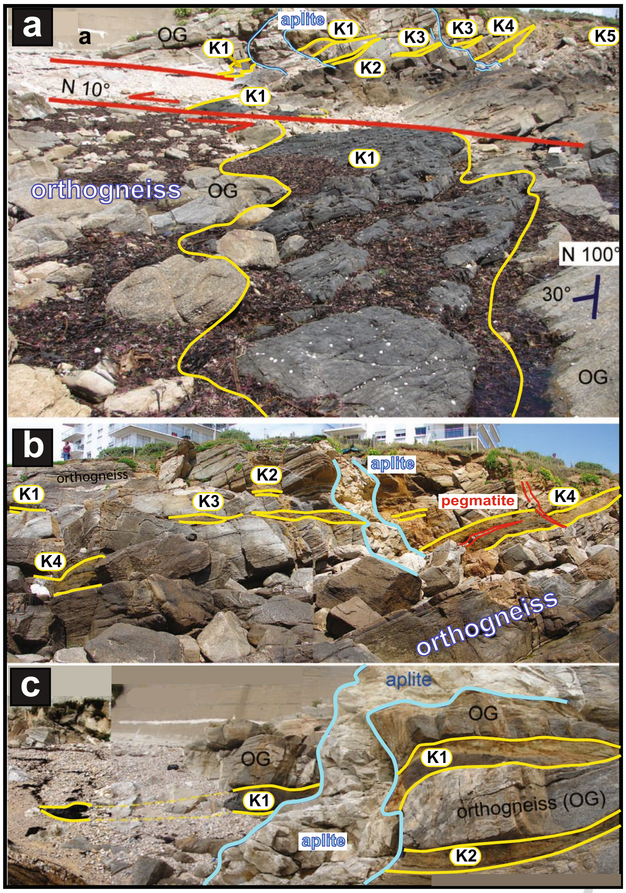

Fig. 4 **a** View of the sills of spessartite (K1 to K5) in the La Chaume cliff and foreshore from West to East. Sills are intruded in the foliation of the orthogneiss (OG). **b** Sills of spessartite in the La Chaume cliff. Slices of pegmatite from the underlying pluton of granite are also intruded in the orthogneiss. Dykes of pegmatite and aplite from the same pluton of granite crosscut all the metamorphic formations. **c** Sills of spessartite in the La Chaume cliff. Orthogneiss and aplite dyke

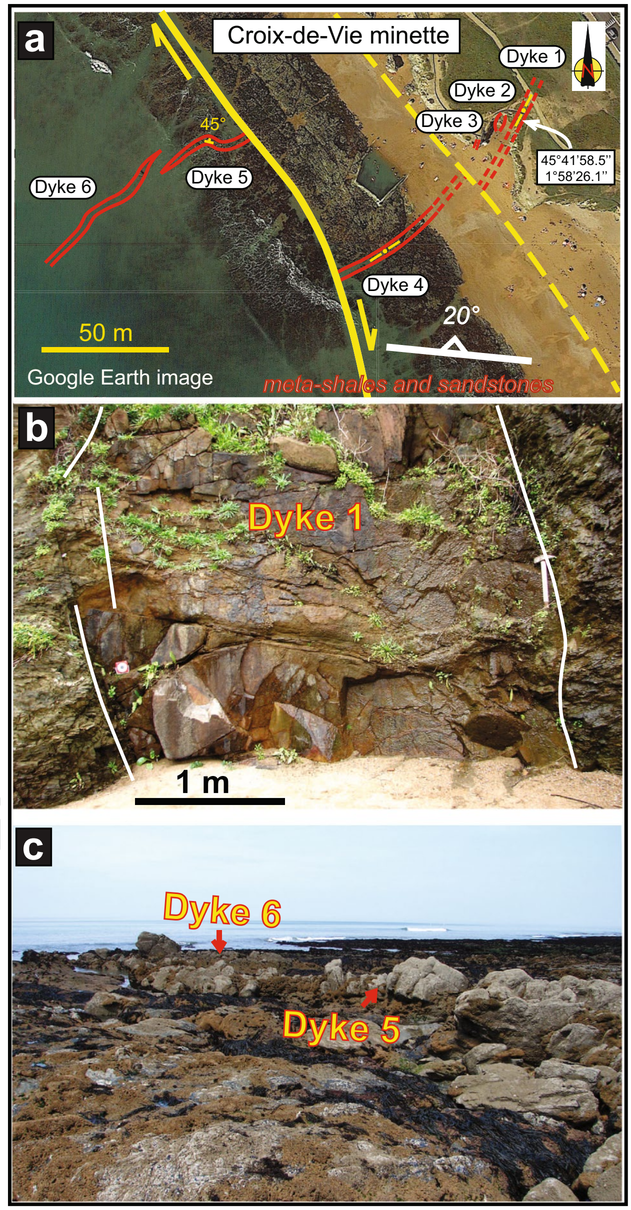

Fig. 5 **a** Sketch map of the Croix-de-Vie sea shore (Google Earth image). Location of the dykes of minette. The two systems of dykes 1, 2, 3 and 4 and of dykes 5 and 6 are 65 m offset by a right-lateral shear zone. Map data Google Earth Image ©2020 Maxar Technologies. Online available at: http://www.google.com/earth/index.html. **b** View of the dyke 1 of minette of Croix-de-Vie, vertically intruded the metasedimentary formations of the cliff. **c** View of the dykes 5 and 6 of minette of Croix-de-Vie. The en echelon dykes cross the foreshore

dipping to the north. They have the composition of minette with fine grain texture and biotite amount similar to that of the Croix-de-Vie minette.

Analytical procedures

Mineral analyses

The minerals were analysed with a CAMECA SX 100 electron probe microanalyser (EPMA) The reference materials were diopside for Si, Ca and Mg, Fe_2O_3 for Fe, $MnTiO_3$ for Ti and Mn, Cr_2O_3 for Cr, albite for Na, orthoclase for K and Al. The Kα X-ray was used for all the elements. The operating conditions were: accelerating voltage of 15 kV and beam current of 10 nA. Counting times were 20 s for the peak and 10 s for the background. Data corrections were made using the PAP method according to Pouchou and Pichoir (1991). Analyses were obtained during six EPMA sessions from June 2016 to June 2018.

Age dating

The minette of Croix-de-Vie has been dated by K–Ar method on the whole rock. The sample was crushed and sieved to

Journal : Large 710 | Article No : 786 | Pages : 25 | MS Code : 786 | Dispatch : 1-7-2022

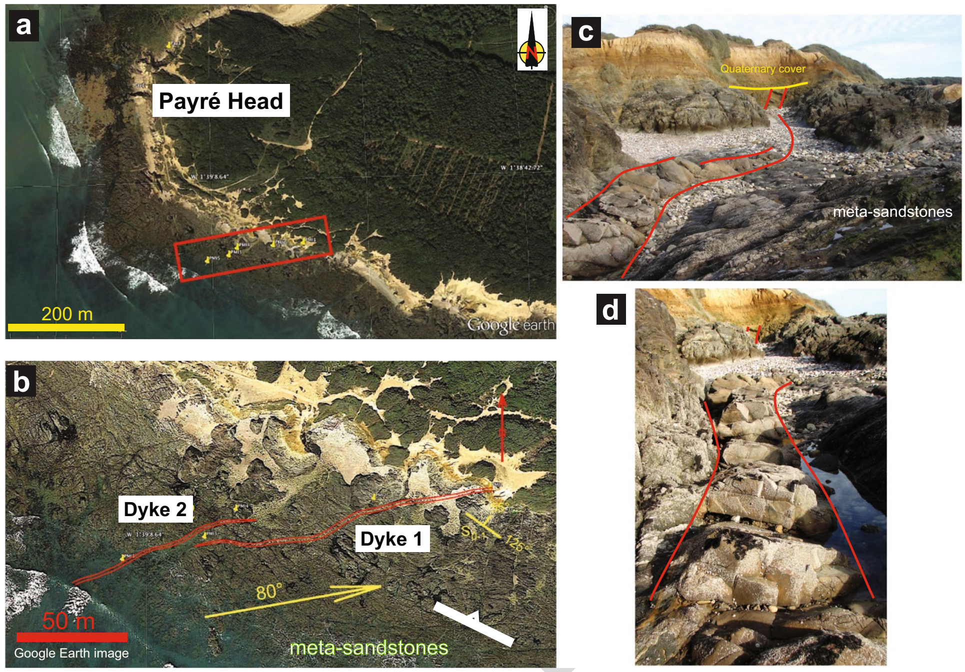

Fig. 6 **a** Sketch map of the Payré Head (Google Earth image). Location of the dykes of minette. **b** Enlarged view of the Payré sea shore (Google Earth image). The echelon dykes 1 and 2 are trending N 80°. **c** View of the dyke #1 of minette on the foreshore and in the cliff of the Payré Head. **d** View of the dyke #1 of minette on the foreshore of the Payré Head. Map data used in subfigures a and b are Google Earth images ©2020 Maxar Technologies, online available at http://www.google.com/earth/index.html

grains of the whole rock (0.3 to 0.18 mm in size), then cleaned with distilled water. One aliquot of grains was powdered in an agate grinder for its chemical attack of around 0.1 g of powder by 4 cc of hydrofluoric acid, before its analysis of K content by AAS (Atomic Absorption Spectrometry). A second aliquot of grains, 0.8 to 1 g, was reserved for argon analysis. Grains were heated and fused under vacuum in a molybdenum crucible, using a high frequency generator. Released gases during this step of the process were cleaned successively on three quartz traps containing titanium sponge during their decreasing temperature, in half a quarter of hour, from 800 °C to the ambient one, and at the final step the remaining gas fraction was ultra-purified with an Al-Zr SAES getter. Isotopic compositions of argon and concentrations of $^{40}Ar^{*}$ were measured in a stainless steel mass spectrometer with a180° geometry. Isotopic dilution was realized during the fusion step, using for this process precise concentrations of ^{38}Ar buried as ions in Al targets, each target being added to the sample before its introduction in the vacuum system for the extraction of gases. Details of the analytical procedure are given in Bellon and Rangin (1991). Constants are from Steiger and Jäger (1977). Uncertainties are calculated following Cox and Dalrymple (1967).

Rock analyses

The spessartite LC has been analysed for major elements by ICP-OES (inductively coupled plasma-optical emission spectrometry) and for minor elements by ICP-MS (inductively coupled plasma-mass spectrometry). The minettes MIT, PMI, and the kersantite KER have been analysed by ICP-OES for major and minor elements. The analytical procedure for the ICP-OES analysis is described in Cotten et al. (1995). For each sample, about 300 mg of powder was fused with $LiBO_2$ and dissolved in HNO_3. Five international geostandards were used: basalt BR, diorite DRN, serpentinite UBN, anorthosite ANG and granite GH. Geostandard references and analytical errors and uncertainties are available in Carignan et al. (2001).

Results: petrography and mineralogy of the West Vendean and West Armorican lamprophyres

Generalities

All the sills of spessartite of La Chaume and the dykes of minette of Croix-de-Vie and of Payré described in Figs. 3, 4, 5 and 6 have been sampled. After elimination of some higher altered rocks, samples were cut for microscope thin sections, and some were selected and polished for electron probe microanalyser (EPMA) analyses. In addition, samples of kersantite have been selected at l'Hôpital-Camfrout from the western Armorican lamprophyre swarm, to support the examination of the various Armorican Domain lamprophyre types. The EPMA provided analyses of magmatic phases: mica, amphibole, feldspar, magnetite, ilmenite, titanite, calcite, and ankerite, and of secondary minerals: chlorite and epidote. Representative chemical analyses are given in the Tables 1, 2, 3, 4, 5 and 6.

Journal : Large 710 | Article No : 786 | Pages : 25 | MS Code : 786 | Dispatch : 1-7-2022

Spessartite of La Chaume

All the sills of La Chaume exhibit the same micrograined and lamprophyric texture with abundant amphibole and biotite. The other phases consist of plagioclase, alkaline feldspars, and accessory ilmenite, apatite, and titanite (Fig. 7a). The modal analysis gives 31% amphibole, 16% biotite, 29% plagioclase, 22% alkaline feldspar, and 2% accessory minerals. According to the IUGS nomenclature of Le Maitre et al. (2005), this lamprophyre is a spessartite in having more amphibole than biotite, more plagioclase than alkaline feldspar, and the lack of feldspathoid. No pyroxene and olivine have been recognized. Secondary alteration gave chlorite, epidote and albite recrystallization of feldspar and amphibole. Biotite is partly changed to muscovite. Many sills are contaminated by xenocrysts of quartz and garnets that are abundant in the gneiss country rocks.

The set of EPMA mineral analyses mainly concerns amphiboles, micas, feldspars and chlorites (Tables 1, 2, 3 and 6). A few data were obtained for oxides and titanite (Table 4). The amphibole compositions range from tschermakitic pargasite to Mg-hornblende with $6.10 < Si_{apfu} < 6.80$ and $0.54 < Mg/Mg + Fe^{2+} < 0.68$ (Table 1), according to the nomenclature of Hawthorne et al. (2012). The amphibole chemistry geobarometer of Ridolfi and Renzulli (2012) applied to the core composition of the more aluminous amphibole gives the value of 712 ± 69 MPa for the pressure of crystallization, by taking the average values of the Eqs. 1b and 1c as suggested by Erdmann et al. (2014). It is the highest value for the amphibole dataset. This pressure would be indicative of a reservoir depth around 26 km for a crustal density of 2.8. The Al-in-hornblende barometer of Ridolfi et al. (2010) gives 668 MPa (Megapascals), which is compatible with the amphibole chemistry barometer. The crystallization temperature is estimated at 840 °C after Ridolfi and Renzulli (2012). According to Molina et al. (2015), the amphibole-liquid Mg partitioning gives 1019 °C and the liquid only gives 1044 °C. The equation of Putirka (2016) for the amphibole-liquid only gives also 1018 °C. These last values seem to be more consistent for a lamprophyric magma at deep crustal setting. The log fO_2 is calculated at -13.3 after Ridolfi and Renzulli (2012).

Table 1 Results of representative chemical analyses of amphiboles of the spessartite of La Chaume

	Tschermakite						Mg-Hornblende					
Major oxides (wt%)												
SiO_2	41.40	42.14	43.23	44.31	43.82	43.07	43.90	44.84	44.66	46.03	45.74	46.41
TiO_2	0.65	0.99	0.98	1.17	1.13	1.08	0.90	0.92	0.93	0.75	0.84	0.80
Al_2O_3	19.76	16.32	14.75	13.37	13.76	12.95	12.64	11.74	11.97	10.67	10.17	9.57
Cr_2O_3	0.08	0.00	0.00	0.00	0.01	0.00	0.00	0.05	0.04	0.00	0.00	0.04
FeO	14.96	16.52	16.81	16.07	17.07	17.61	17.53	17.24	17.01	16.25	17.12	16.61
MnO	0.28	0.24	0.23	0.25	0.22	0.22	0.25	0.24	0.27	0.31	0.24	0.28
MgO	9.62	9.18	9.18	9.83	9.03	8.99	9.76	10.02	9.64	10.89	10.46	10.90
CaO	10.12	10.73	11.04	10.86	11.34	11.07	11.25	11.21	11.13	11.25	11.14	11.46
Na_2O	0.87	1.30	1.34	1.19	1.56	1.47	1.44	1.26	1.34	1.04	1.29	1.09
K_2O	0.32	0.48	0.57	0.35	0.65	0.65	0.54	0.41	0.44	0.26	0.39	0.34
Total	98.06	97.90	98.15	97.40	98.58	97.10	98.20	97.93	97.42	97.44	97.38	97.51
Calculated mineral formulae (apfu)*												
Si	5.830	6.099	6.294	6.455	6.414	6.403	6.420	6.552	6.573	6.705	6.721	6.802
Al^{IV}	2.170	1.901	1.706	1.545	1.586	1.597	1.580	1.448	1.427	1.295	1.279	1.198
Al^{VI}	1.109	0.883	0.825	0.749	0.789	0.672	0.599	0.574	0.651	0.536	0.482	0.455
Ti	0.069	0.107	0.108	0.128	0.124	0.120	0.099	0.101	0.103	0.082	0.093	0.088
Cr	0.009	0.000	0.000	0.000	0.001	0.000	0.000	0.005	0.004	0.000	0.000	0.005
Mn	0.033	0.029	0.029	0.031	0.027	0.027	0.031	0.030	0.034	0.038	0.030	0.035
Fe^{3+}	1.514	0.998	0.723	0.737	0.423	0.604	0.735	0.710	0.583	0.730	0.655	0.584
Fe^{2+}	0.247	1.003	1.324	1.221	1.666	1.586	1.410	1.397	1.511	1.249	1.449	1.453
Mg	2.019	1.980	1.991	2.133	1.970	1.991	2.127	2.183	2.115	2.365	2.292	2.381
Na	0.238	0.366	0.379	0.336	0.444	0.424	0.408	0.357	0.382	0.293	0.367	0.309
K	0.058	0.090	0.106	0.065	0.120	0.123	0.100	0.076	0.083	0.048	0.073	0.064
Ca	1.526	1.664	1.723	1.695	1.778	1.763	1.764	1.756	1.755	1.756	1.753	1.799
Total	14.822	15.119	15.208	15.096	15.343	15.309	15.273	15.190	15.220	15.097	15.194	15.172

*calculated based on 23 O atoms per formula unit

Journal : Large 710	Article No : 786	Pages : 25	MS Code : 786	Dispatch : 1-7-2022

Table 2 Results of representative chemical analyses of micas

Sample	Spessartite LCS-3			Minette MIT					Minette MIT-2			
Major oxides (wt%)												
SiO_2	32.97	35.22	36.12	35.48	35.33	37.59	39.88	38.58	39.13	38.95	39.74	35.15
TiO_2	2.56	2.98	3.20	3.40	3.92	3.94	2.32	3.58	2.17	2.05	2.72	4.80
Al_2O_3	25.15	24.52	24.10	13.97	14.85	14.78	13.64	14.58	14.49	14.86	14.37	15.84
FeO	16.06	15.40	15.66	12.91	14.32	9.03	5.46	10.99	5.00	4.58	5.66	19.00
MnO	0.07	0.08	0.09	0.10	0.17	0.08	0.00	0.03	0.00	0.02	0.05	0.04
MgO	9.43	8.55	8.44	16.21	14.49	18.95	22.58	17.38	22.34	22.25	22.39	11.45
CaO	0.50	0.19	0.20	1.61	0.03	0.00	0.00	0.09	0.00	0.00	0.01	0.06
Na_2O	0.11	0.36	0.22	0.46	0.46	0.44	0.20	0.55	0.20	0.24	0.16	0.39
K_2O	8.27	7.20	7.02	8.00	8.06	8.90	9.56	8.15	8.89	9.08	8.87	6.64
BaO	0.07	0.06	0.04	1.55	2.12	1.71	0.76	1.36	0.72	0.77	0.80	2.48
Total	95.18	94.56	95.09	93.69	93.74	95.42	94.38	95.30	92.95	92.79	94.78	95.84
Calculated mineral formulae (apfu)*												
Si	2.455	2.598	2.643	2.727	2.734	2.771	2.877	2.841	2.824	2.804	2.849	2.700
Al^{IV}	1.545	1.402	1.357	1.266	1.266	1.229	1.123	1.159	1.176	1.196	1.151	1.300
Al^{VI}	0.662	0.730	0.721	0.000	0.088	0.055	0.036	0.106	0.057	0.064	0.064	0.134
Ti	0.144	0.165	0.176	0.197	0.228	0.218	0.126	0.198	0.118	0.111	0.147	0.277
Fe	1.000	0.950	0.958	0.830	0.927	0.557	0.330	0.677	0.302	0.276	0.339	1.220
Mn	0.004	0.005	0.006	0.007	0.011	0.005	0.000	0.002	0.000	0.001	0.003	0.003
Mg	1.047	0.940	0.921	1.857	1.671	2.083	2.428	1.908	2.404	2.387	2.393	1.311
K	0.787	0.679	0.657	0.786	0.797	0.838	0.881	0.767	0.820	0.836	0.813	0.652
Na	0.015	0.051	0.031	0.068	0.069	0.063	0.027	0.079	0.028	0.033	0.023	0.058
Ba	0.002	0.002	0.001	0.047	0.064	0.049	0.021	0.039	0.020	0.022	0.023	0.075
Major oxides (wt%)												
SiO_2	38.21	38.68	37.92	37.59	38.48	36.80	38.40	36.84	36.50	35.63	35.92	33.90
TiO_2	4.65	4.19	4.59	4.72	4.68	4.87	4.27	2.54	2.93	2.13	2.38	3.26
Al_2O_3	14.22	13.87	14.30	14.28	14.19	14.42	14.36	15.88	15.82	17.57	16.19	18.85
FeO	6.96	6.61	6.83	9.43	6.92	14.40	6.62	12.30	18.15	16.48	13.20	11.83
MnO	0.12	0.01	0.01	0.08	0.01	0.26	0.06	0.00	0.00	0.09	0.16	0.07
MgO	20.12	20.30	19.98	18.03	20.10	14.90	20.36	19.55	13.55	13.86	18.69	19.52
Na_2O	0.50	0.45	0.48	0.44	0.46	0.52	0.46	0.74	0.71	0.59	0.68	0.83
K_2O	9.35	9.37	9.29	9.38	9.36	8.96	9.41	8.00	7.80	8.66	7.90	8.13
BaO	0.64	0.45	0.41	0.64	0.57	0.70	0.57	0.00	0.00	0.00	0.00	0.00
Total	94.76	93.92	93.80	94.59	94.76	95.83	94.50	95.85	95.46	95.01	95.12	96.39
Calculated mineral formulae (apfu)*												
Si	2.782	2.819	2.779	2.770	2.789	2.744	2.789	2.687	2.742	2.682	2.656	2.468
Al^{IV}	1.218	1.181	1.221	1.230	1.211	1.256	1.211	1.313	1.258	1.318	1.344	1.532
Al^{VI}	0.003	0.011	0.014	0.011	0.001	0.012	0.018	0.052	0.143	0.240	0.066	0.086
Ti	0.255	0.230	0.253	0.262	0.255	0.273	0.233	0.139	0.166	0.121	0.132	0.179
Fe	0.424	0.403	0.418	0.581	0.419	0.898	0.402	0.750	1.140	1.037	0.816	0.720
Mn	0.007	0.000	0.001	0.005	0.000	0.017	0.003	0.000	0.000	0.006	0.010	0.004
Mg	2.183	2.206	2.183	1.980	2.172	1.656	2.203	2.125	1.517	1.555	2.060	2.119
K	0.870	0.873	0.870	0.884	0.867	0.855	0.874	0.746	0.749	0.833	0.747	0.757
Na	0.071	0.064	0.068	0.062	0.065	0.075	0.065	0.105	0.103	0.086	0.097	0.117
Ba	0.018	0.013	0.012	0.018	0.016	0.020	0.016	0.000	0.000	0.000	0.000	0.000

*calculated based on 11 O atoms per formula unit

Journal : Large 710 | Article No : 786 | Pages : 25 | MS Code : 786 | Dispatch : 1-7-2022

Table 3 Results of representative chemical analyses of feldspars

Sample	Spessartite LCS					Minette MIT		Minette PMI			Kersantite KER	
Major oxides (wt%)												
SiO_2	59.63	59.35	59.29	60.07	60.72	65.55	65.23	59.10	59.90	60.56	54.42	57.84
Al_2O_3	25.85	25.58	25.47	25.56	25.13	18.54	18.78	24.99	25.02	24.10	27.95	24.77
Fe_2O_3	0.25	0.13	0.09	0.02	0.03	0.35	0.37	0.36	0.28	0.46	0.94	0.21
CaO	7.06	6.99	6.94	6.76	6.29	0.16	0.29	6.75	6.55	6.56	12.21	10.98
Na_2O	7.64	7.63	7.66	7.89	8.18	2.44	2.55	7.04	7.33	7.12	4.41	5.24
K_2O	0.07	0.13	0.13	0.12	0.08	12.86	12.92	1.02	0.52	1.33	0.11	0.04
Total	100.50	99.81	99.59	100.42	100.44	99.90	100.14	99.26	99.60	100.13	100.04	99.08
Calculated mineral formulae (apfu)*												
Si	2.646	2.652	2.655	2.665	2.689	2.996	2.980	2.664	2.680	2.706	2.463	2.620
Al	1.352	1.347	1.344	1.336	1.312	0.999	1.011	1.328	1.319	1.269	1.491	1.323
Fe^{3+}	0.008	0.004	0.003	0.001	0.001	0.012	0.013	0.012	0.009	0.015	0.032	0.007
Ca	0.336	0.335	0.333	0.321	0.299	0.008	0.014	0.326	0.314	0.314	0.592	0.533
Na	0.657	0.661	0.665	0.679	0.703	0.216	0.226	0.615	0.636	0.617	0.387	0.460
K	0.004	0.007	0.007	0.007	0.005	0.752	0.755	0.059	0.030	0.076	0.006	0.002
Calculated end-member fractions (mol%)												
Ab	65.93	65.89	66.15	67.42	69.86	22.17	22.71	61.52	64.91	61.26	39.27	46.24
An	33.65	33.36	33.11	31.92	29.69	0.79	1.42	32.60	32.05	31.19	60.08	53.54
Or	0.41	0.74	0.74	0.66	0.46	77.04	75.87	5.88	3.04	7.55	0.65	0.22

*calculated based on 8 O atoms per formula unit

However, these estimated crystallization conditions have to be taken with caution, as noted by Molina et al. (2021). Only few analyses were available for biotite, because of the secondary substitution in muscovite of the magmatic biotite (Table 2). They comply with an alumina-rich biotite of eastonite close to siderophyllite composition with the Mg/Mg + Fe^{2+} ratio averaging 51 according to the nomenclature of Rieder et al. (1998). Partition of titanium between melt

Table 4 Results of representative chemical analyses of titanites

Sample	Spessartite LCS3		Kersantite KER 1				
Major oxides (wt%)							
SiO_2	29.80	30.12	31.04	30.55	30.73	29.47	29.75
TiO_2	36.24	34.22	28.36	29.33	28.65	33.72	32.01
Al_2O_3	4.28	4.28	8.62	8.04	7.94	3.99	6.27
Cr_2O_3	0.02	0.03	0.16	0.01	0.10	0.06	0.04
FeO	1.10	0.88	0.37	0.32	0.44	0.81	1.07
MnO	0.00	0.00	0.00	0.00	0.04	0.00	0.06
MgO	0.00	0.00	0.00	0.02	0.01	0.09	1.33
CaO	27.51	28.66	28.76	28.80	28.80	27.40	25.79
Total	98.95	98.19	97.31	97.08	96.71	95.54	96.31
Calculated mineral formulae (apfu)*							
Si	3.919	3.996	4.104	4.057	4.098	4.011	3.985
Al	0.663	0.669	1.343	1.259	1.249	0.640	0.989
Ti	3.584	3.414	2.819	2.929	2.873	3.451	3.224
Fe^{2+}	0.121	0.098	0.041	0.035	0.049	0.092	0.120
Mg	0.000	0.000	0.000	0.004	0.002	0.017	0.265
Mn	0.000	0.000	0.000	0.000	0.004	0.000	0.006
Cr	0.002	0.003	0.016	0.001	0.011	0.007	0.004
Ca	3.877	4.074	4.074	4.098	4.114	3.996	3.701

*calculated based on 20 O atoms per formula unit

Table 5 Results of representative chemical analyses of ankerite of the minettes

Sample	MIT		PMI	
Major oxides (wt%)				
SiO_2	0.17	0.22	1.39	0.04
TiO_2	0.01	0.00	0.00	0.00
Al_2O_3	0.02	1.71	0.52	0.05
FeO	6.43	4.50	6.90	5.67
MnO	0.67	0.81	0.45	0.57
MgO	15.38	16.19	14.74	17.98
CaO	28.54	29.82	29.28	29.10
Na_2O	0.00	0.00	0.00	0.03
K_2O	0.04	0.08	0.33	0.02
Total	51.27	53.34	53.62	53.47
CO_2*	46.00	46.00	46.00	46.00
Calculated mineral formulae (apfu)**				
Si	0.006	0.007	0.046	0.001
Ti	0.000	0.000	0.000	0.000
Al	0.001	0.065	0.020	0.002
Fe	0.179	0.121	0.189	0.155
Mn	0.019	0.022	0.013	0.016
Mg	0.764	0.776	0.719	0.876
Ca	1.019	1.027	1.026	1.019
Calculated end-member fractions (mol%)				
Calcite	12.88	12.91	15.80	6.93
Dolomite	77.12	79.74	73.86	84.80
Siderite	9.04	6.22	9.70	7.50
Rhodonite	0.95	1.13	0.64	0.76

*average of calculated values; **calculated based on 6 O atoms per formula unit

and magnesium biotite is temperature dependent. Using the geothermometer of Righter and Carmichael (1996) with the revised constants of Roach and Rutherford (2003), the biotite was equilibrated at 1140 °C, which can be compared with the 1018 °C-1044°C values of the amphibole crystallization. Plagioclase is in the labradorite range (An_{66-72}) (Table 3). The alkaline feldspar composition averages Ab 65% and Or 35%. Titanite contains 36% TiO_2 and 28% CaO (Table 4). Chlorite ranges from ripidolite to pycnochlorite ($5.2 < Si_{apfu} < 5.7$; $0.52 < Fe/Fe + Mg < 0.54$) (Table 6) in the nomenclature of Hey (1954) reviewed by Bayliss (1975). According to the Zang and Fyfe's (1995) thermometer, the chlorite crystallized around 250 °C. This high temperature indicates a local thermal effect from hot country rocks.

Minettes of Croix-de-Vie and Payré

Lamprophyres of Croix-de-Vie and Payré dykes display the same textural and mineral compositions. They show a microporphyritic micrograined texture rich in mica and alkaline feldspars in a fine grained felsic groundmass (Fig. 7b and c). In some parts, aggregated flakes of biotite mimic a lamprophyric texture. There are no significant grain size variations from core to margin of the intrusive bodies. The feldspar microphenocrysts and microcrysts consist of microcline-orthoclase with pericline and albite twins. The groundmass is made of microcrysts of biotite, microcline, quartz, magnetite, scarce amphibole and rare zircon, plus needles of apatite and few aggregates of ankerite-calcite. Apatite and zircons can be included in mica. We did not observe any pyroxene or olivine crystals.

The average modal composition of the Croix-de-Vie rock is: 44% feldspar, 34% biotite, 21% quartz, and 1% accessory minerals of magnetite, apatite and zircon. For the Payré rock, the composition is: 48% feldspar, 34% biotite, 17% quartz, and 1% accessory minerals. It is slightly richer in feldspar and less siliceous than the Croix-de-Vie rock. These compositions that are rich in biotite and alkaline feldspar clearly fit with a minette lamprophyre (Rock 1987, 1991; Le Maitre et al. 2005).

EPMA analyses were done for amphibole, biotite, feldspar, carbonate and chlorite. Rare amphiboles are determined as cummingtonite. The biotite is Al- and Mg-rich and plots close do the eastonite end-member in the Mg-Fe-Al diagram (Table 2) ($0.53 < Mg/Mg + Fe^{2+} < 0.88$). It is moderately titaniferous and has low Ba contents ($2.3 < TiO_2$ wt% < 5.6; $0.5 < BaO < 2.1$). The large crystals are zoned with Ti, Fe and Ba enrichments from core to the margin. This zonation is explained by decreasing temperature during crystallization (Righter and Carmichael 1996). Using the TiO_2 geothermometer of Righter and Carmichael (1996) with the revised constants of Roach and Rutherford (2003), biotite of the Croix-de-Vie minette is equilibrated between 948 and 1009 °C, and biotite of Payré between 969 and 984 °C. The feldspar compositions range from Or 91 to 80 for phenocrysts and from Or 80 to 68 for microcrysts. This variation witnesses the increasing Na content in the crystallization course. The anorthite content is low, 0.8 – 3.4%. BaO is less than 0.8%. Microphenocrysts and microcrysts of magnetite are moderately Ti-enriched ($5.1 < TiO_2$ wt% < 5.3) with the end member contents of 78 < Magnetite % < 80, 15 < Ulvospinel % < 16, and 5 < Hercynite % < 6. An ankeritic carbonate was analysed in the matrix of both Croix-de-Vie and Payré minettes (19 < calcite % < 28; 57 < dolomite % < 68; 11 < siderite % < 13). During alteration processes, feldspars gained albitized margins and biotites were partly changed to muscovite. Secondary minerals in the groundmass consist of quartz, albite, calcite, epidote, chlorite, hydromuscovite, and hematite. Chlorites are in the picnochlorite to diabantite range ($5.7 < Si_{apfu} < 6.7$; $0.28 < Fe/Fe + Mg < 0.46$). These chlorites may have crystallized around 200 °C according to the Zang and Fyfe's (1995) thermometer.

Journal : Large 710 | Article No : 786 | Pages : 25 | MS Code : 786 | Dispatch : 1-7-2022

Table 6 Results of representative chemical analyses of chlorites

Sample	Spessartite K1LC			Minette MIT-2				Minette PMI		Kersantite KER-1				
	rip	rip	pyc	pyc	pyc	dia	dia	pyc	dia	pyc	pyc	pyc	dia	dia
Major oxides (wt%)														
SiO_2	25.25	26.93	24.84	29.19	28.53	31.76	31.74	28.13	33.10	26.39	27.81	27.63	29.20	32.04
TiO_2	0.06	0.20	0.02	0.20	0.12	0.04	0.03	0.00	0.12	0.29	0.35	0.07	0.00	0.01
Al_2O_3	26.35	25.01	19.97	28.87	16.59	17.67	18.08	22.21	21.57	15.49	19.35	16.30	17.22	17.33
Cr_2O_3	0.10	0.00	0.03	0.05	0.04	0.02	0.03	0.06	0.15	0.14	0.07	0.04	0.13	0.12
FeO	23.68	23.63	24.35	18.35	18.54	15.60	18.90	21.39	13.54	17.57	18.93	19.58	18.06	15.95
MnO	0.13	0.11	0.19	0.07	0.02	0.02	0.07	0.08	0.04	0.22	0.27	0.18	0.20	0.18
MgO	11.40	12.42	11.46	11.96	20.72	22.35	19.62	15.03	14.76	22.50	18.80	20.48	21.23	21.6
CaO	1.25	0.35	0.38	0.35	0.43	0.20	0.35	0.37	0.50	0.41	0.21	0.10	0.20	0.21
Na_2O	0.01	0.01	0.04	0.04	0.02	0.04	0.00	0.01	0.00	0.00	0.01	0.01	0.00	0.03
K_2O	0.05	0.02	0.15	0.29	0.01	0.03	0.02	0.03	0.18	0.10	0.20	0.01	0.00	1.03
Total	88.28	88.69	81.43	89.37	85.02	87.73	88.84	87.31	83.97	83.11	85.98	84.40	86.23	88.50
Calculated mineral formulae (apfu)*														
Si	5.215	5.498	5.645	5.691	5.982	6.284	6.302	5.775	6.681	5.698	5.773	5.887	6.006	6.340
Ti	0.009	0.030	0.003	0.030	0.018	0.006	0.004	0.000	0.018	0.046	0.055	0.011	0.000	0.002
Al	6.415	6.018	5.350	6.635	4.102	4.122	4.231	5.375	5.131	3.942	4.734	4.093	4.175	4.042
Fe	4.090	4.035	4.629	2.992	3.252	2.581	3.139	3.673	2.286	3.172	3.287	3.489	3.106	2.641
Mn	0.023	0.019	0.037	0.011	0.003	0.004	0.012	0.013	0.006	0.040	0.047	0.032	0.034	0.030
Mg	3.510	3.781	3.883	3.476	6.476	6.593	5.808	4.600	4.442	7.243	5.817	6.504	6.509	6.373
Ca	0.277	0.077	0.092	0.073	0.097	0.041	0.075	0.082	0.109	0.096	0.047	0.024	0.045	0.044
Na	0.003	0.003	0.017	0.014	0.010	0.016	0.000	0.003	0.002	0.000	0.005	0.003	0.000	0.011
K	0.012	0.005	0.044	0.072	0.003	0.008	0.005	0.009	0.046	0.026	0.052	0.004	0.001	0.261
Cr	0.016	0.000	0.005	0.008	0.007	0.003	0.004	0.010	0.025	0.023	0.011	0.007	0.021	0.019

Chlorite names: *rip* ripidolite, *pyc* pycnochlorite, *dia* diabantite

*calculated based on 28 O atoms per formula unit

A few centimetre-sized xenoliths from the host rocks (shales and sandstones) are common in dyke margins. In the middle parts of the intrusions, xenocrysts from the host-rocks are limited to rounded quartz and to rare grains of cordierite (Fe/Fe + Mg X% = 26.9) in the Payré dyke.

Kersantite of l'Hôpital-Camfrout

The thick lode of l'Hôpital-Camfout is representative of the intrusive swarm of kersantite of the Daoulas district of the "Rade de Brest" area, to the western end of Brittany. About one hundred of sills and dykes are intruded in the Upper Devonian sedimentary formations with a thickness of 1 to 20 m and trending N 50° to N 100° (Caroff et al. 2021, Fig. 2). The country rocks were folded and low-grade metamorphosed in the late Devonian to Early Carboniferous. But the lamprophyres did not undergo any metamorphism. The calcic composition of abundant plagioclase phenocrysts allows for distinguishing kersantite and minette in between the mica-rich lamprophyres. The kersantite term has been given from the referring site of Kersanton close to l'Hôpital-Camfrout.

The studied selected sample displays a microporphyritic, micrograined to grained and lamprophyric texture caused by abundant flakes of biotites and platy crystals of amphiboles with feldspars and rare pyroxenes (Fig. 7 d). Biotite is aluminous and magnesian but too much altered for giving accurate analyses. Fortunately, separated biotite flakes from this lode and from neighbouring sills and dykes of the same swarm have been analysed by Velde (1969, 1971) and by Caroff et al. (2021). The biotites of kersantite have compositions close to those of the Vendean minette thought slightly more ferrous, with the exception of higher titanium contents. Amphiboles range from magnesio-hastingsite to tschermakite (Caroff et al., 2021). Pyroxene is lacking in the studied sample, but occurs in neighbouring lodes and have been analysed by Caroff et al. (2021) as augite/diopside. Feldspar phenocrysts have a labradorite composition (An 60–67) (Table 3). Feldspar microcrysts are more sodic plagioclases and are associated with potassic alkaline feldspars. The magmatic paragenesis is completed with microcrysts of titanite ($28.4 < TiO_2 < 32.0$;

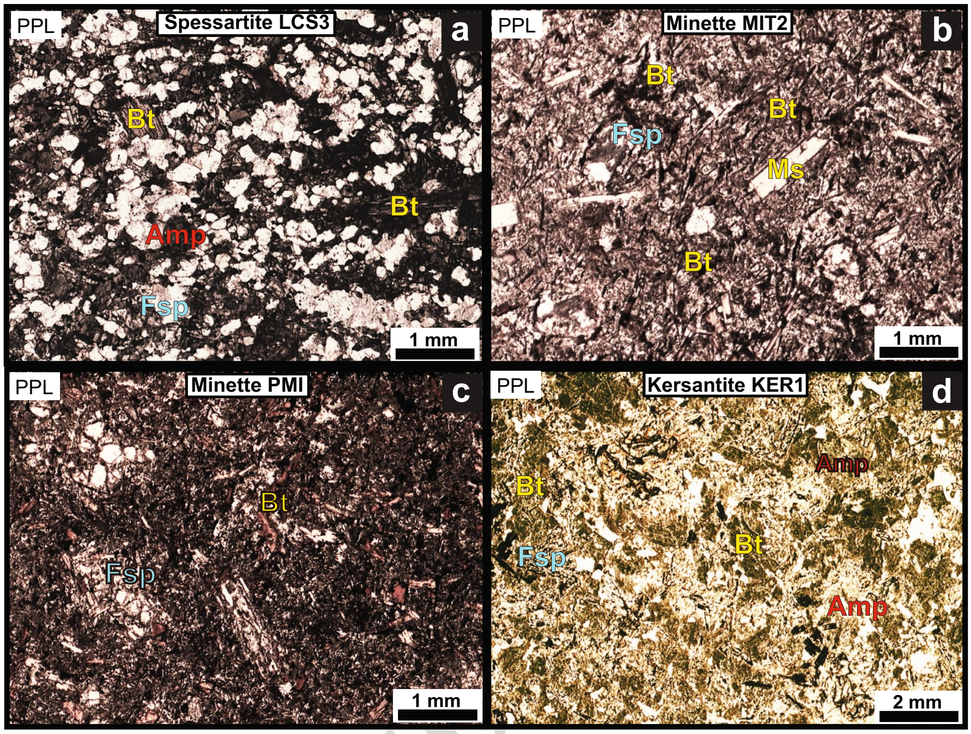

Fig. 7 Photographs of thin section under plane-polarized transmitted-light (PPL). **a** Spessartite LC3. **b** Minette MIT2. **c** Minette PMI. **d** Kersantite KER. Amp, ampbibole; Bt, biotite; Fsp, feldspar; Ms, muscovite

25.8 < CaO < 28.8), apatite, allanite, and magnetite. The secondary mineralogy consists of quartz, albite, epidote (clinozoisite 77–83%, pistacite 17–23%), chlorites and calcite. Chlorites are in the picnochlorite to diabantite range ($5.7 < Si_{apfu} < 6.3$; 0.29 < Fe/Fe + Mg < 0.36) (Table 6). They may have crystallized between 230 °C and 250 °C according to the Zang and Fyfe's (1995) thermometer.

Age of lamprophyre settings

The spessartite sills of La Chaume are contemporaneous with the pegmatites of the granite the age of which is determined ca. 320 Ma (Turillot et al. 2011). The pegmatites resulted from the pneumatolytic stage that followed the crystallization of the pluton. The spessartite intrusions benefited of the fracturing conditions created by the hydraulic pressure of pegmatitic fluids.

Minette dykes of Croix-de-Vie and Payré clearly post-dated the late Variscan metamorphic and folding events. The Croix-de-Vie dykes intruded the tectonic nappe of St-Gilles-sur-Vie that thrust in the Early Late Carboniferous time, and even the post-thrust folds of this nappe, which resulted from a late Carboniferous transpressional event (Pouclet et al. 2017). In return, the dykes are cross-cut by the great NNW-SSE right-lateral strike-slip system of transcurrent faults that took place during the Permian period.

K–Ar dating of the dyke #1 of Croix-de-Vie has been performed on the whole rock. The result is 286.2 ± 6.6 Ma, an Artinskian age in the Early Permian (Table 7). Taking into account the high loss on ignition (5.67%) of the chemical analysis, we proceeded to a mild acid washing to remove altered products. The obtained age is considered to be accurate.

Kersantite of l'Hôpital-Camfrout postdates the Late Devonian metamorphism and folding. A neighbouring and similar lode has been dated by K–Ar at 282 ± 4 Ma (Leutwein et al. 1969). However, another dyke (Bellec Cape) is dated at 254 ± 10 Ma by the same method (Leutwein et al. 1972). According to the authors of the dating, the younger ages may be biased by high alteration of the analysed sample. Taking into account the ages of the tectonic events and the ages of neighbouring magmatic activities, Caroff et al (2021) dated the genesis of the western Armorica kersantites between 330 and 310 Ma. This age coincides with that of the La Chaume spessartite.

Table 7 K/Ar dating result for the minette of Croix-de-Vie

Sample	Mass of sample fused (g)	K_2O (wt. %)	$^{40}Ar^*$ 10^{-5} cm^3/g	$^{40}Ar^*/^{40}Ar_T$ (%)	^{36}Ar $10^{-9}cm^3$	Age (Ma)	±	error (±1 s)
B7599-2	0.3021	6.48	6.479	96.4	2.46	286.2	±	6.6

Journal : Large 710 | Article No : 786 | Pages : 25 | MS Code : 786 | Dispatch : 1-7-2022

Geochemical compositions

The analytical data comprises the sill #1 of La Chaume, the dyke #1 of Croix-de-Vie, the dyke #1 of Payré, and the sill of l'Hôpital-Camfrout (Tables 8 and 9).

A set of analytical data has been collected for lamprophyres of the whole Variscan Belt. Attention has been paid for spessartite-vogesite, minette and kersantite, the common calc-alkaline lamprophyres, with the addition of camptonite, an alkaline lamprophyre distributed in the Spanish Variscan area. In some papers, vogesites are not distinguished from spessartites. Then, they were gathered in our work. Analyses are plotted in the $Na_2O + K_2O$ versus SiO_2 or TAS diagram, the K_2O versus SiO_2, and the K_2O versus Na_2O diagrams (Fig. 8), in order to show the compositional areas of the lamprophyre types. Calc-alkaline lamprophyres plot in the basalt to trachy-andesite fields. Alkaline lamprophyres plot in the basanites field. Spessartites-vogesites are distinguished from other lamprophyres by a fairly more sodic composition. Kersantites show intermediate sodic and potassic compositions. Minettes are potassic to perpotassic with a K_2O/Na_2O ratio higher than 2.4.

The spessartite of La Chaume (LC) is a basic rock (47 wt% SiO_2) plotting in the basalt field (Fig. 8a). It is slightly titaniferous and magnesian (2.7 wt% TiO_2; 5.7 wt% MgO) but rich in iron (11.6 wt% FeO^t). For this last reason, the Mg number is low in spite of the mafic composition (molar 100 Mg/Mg + Fe^{2+} or Mg number = 49.6). Alkali contents are moderate with a major sodic content (3.4 wt% Na_2O; 1.3 wt% K_2O) (Fig. 8c). The norm composition is saturated with 15.3 Ol and the lack of Qtz and Ne. The loss on ignition (LOI) is low (1.7) precluding any alteration effect. Compatible minor element contents are low (186 ppm; V; 20.3 Cr; 37.5 Co; 65.8 Ni; 46.4 Cu;

Table 8 Results of major element chemical analyses of the lamprophyres

Location	La Chaume	Croix-de-Vie	Payré	L'Hopital-Camfrout
Sample	LC	MIT	PMI	KER
Setting	sill #1	dyke #1	dyke #1	sill
Petrography	Spessartite	Minette	Minette	Kersantite
Oxides (wt%)				
SiO_2	47.06	57.00	52.60	56.30
TiO_2	2.71	0.77	1.17	1.00
Al_2O_3	15.84	13.30	13.80	15.30
Fe_2O_3	12.92	4.70	4.70	6.20
MnO	0.19	0.12	0.10	0.08
MgO	5.65	5.03	5.72	6.36
CaO	7.66	3.86	4.99	3.91
Na_2O	3.40	2.98	1.46	3.16
K_2O	1.33	4.62	6.48	3.17
P_2O_5	0.34	0.80	0.56	0.33
LOI	1.69	5.67	7.97	4.91
Total	98.77	98.85	99.55	100.72

Table 9 Results of minor element chemical analyses of the lamprophyres

Sample	LC	MIT	PMI	KER
Be	1.01			
Sc	21.3			
V	186	93	123	137
Cr	20.3	258	252	318
Co	37.5	21.4	19.9	14.0
Ni	65.8	133.1	153.3	68.6
Cu	46.4			
Zn	121			
Ga	22.2			
Ge	1.32			
As	6.77			
Rb	44.3	171	265	106
Sr	398	1675	452	476
Y	27.2	27.9	28.3	20.6
Zr	188	510	636	256
Nb	18.4	24.4	29.9	13.7
Mo	0.69			
Cd	0.19			
Sn	3.72			
Sb	0.46			
Cs	1.40			
Ba	858	3735	1404	2240
Hf	4.81			
Ta	1.45			
Pb	3.57			
Bi	0.12			
Th	1.48	36.7	19.0	24.9
U	0.60			
La	10.50	69.2	71.1	46.5
Ce	29.10	145.0	145.6	92.8
Pr	4.12			
Nd	20.30	71.3	65.7	44.5
Sm	5.83	13.5	11.5	8.0
Eu	2.17	3.28	2.88	2.13
Gd	5.93	9.3	8.4	5.4
Tb	0.95			
Dy	5.74	5.4	5.4	3.9
Ho	1.08			
Er	2.71	2.0	2.1	2.0
Tm	0.36			
Yb	2.22	1.92	1.85	1.76
Lu	0.32			

All values are quoted in ppm

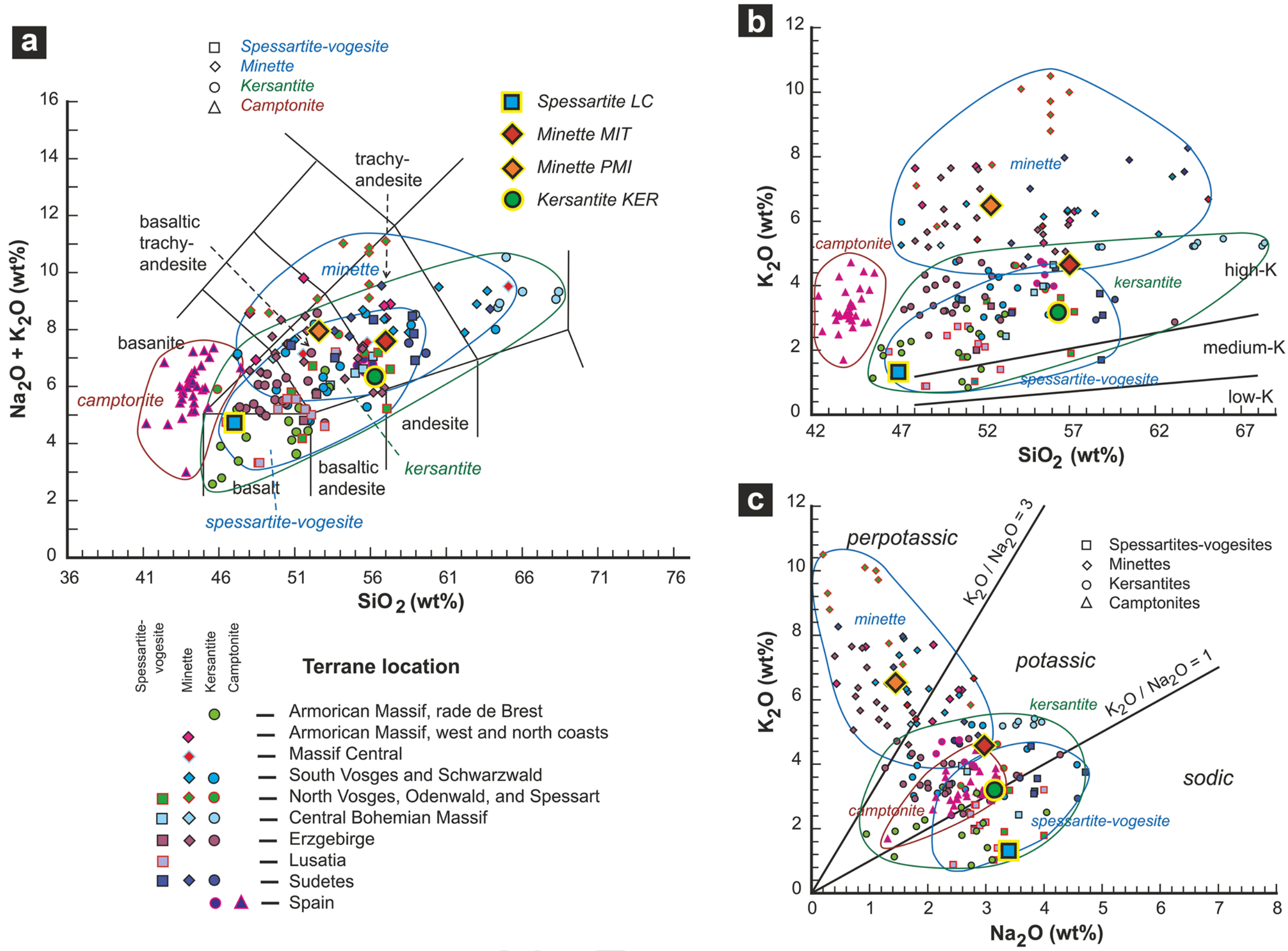

Fig. 8 **a** Na_2O+K_2O versus SiO_2 or TAS diagram (total alkali-silica). The compositional areas of spessartites-vogesites (squares), minettes (diamonds), kersantites (circles), and camptonites (triangles) are drawn after an analytical set of Variscan lamprophyres with data from Turpin et al. (1988), Wagner et al. (1992), Chauris and Hallégouët (1994), Durand-Delga et al. (1997), Hegner et al. (1998), von Seckendorff et al. (2004), Awdankiewicz (2007), Orejana et al. (2008), Seifert (2008), Scarrow et al. (2011), Abdelfadil (2013), Štemprok et al. (2014), Caroff et al. (2015), Soder and Romer (2018). The terrane location of lamprophyres is shown by the colours of symbols. Studied samples are highlighted by larger symbols. We use raw data without recalculation to 100% free of H_2O and CO_2. Comparison with fields of the nomenclature is thus a rough estimate. **b** K_2O versus SiO_2 diagram. Minettes are well discriminated by their high potassic content. Kersantites are moderately potassic. Camptonites are also moderately potassic and distinguished by their low silica content. **c** K_2O versus Na_2O diagram. Spessartites-vogesites are fairly more sodic than kersantites

121 Zn; 3.2 Sn; 3.6 Pb), indicating that this lamprophyre is not a primary mantle melt but underwent fractionation, as also shown by the high iron content. Lithophile and high field strength elements are low (1 ppm Be; 398 Sr; 1.4 Cs; 1.5 Th; 0.6 U; 27.2 Y; 188 Zr; 4.8 Hf; 18.4 Nb, 1.5 Ta) except Rb and Ba (44.3 Rb; 858 Ba). Rare earth elements (REE) are also low and fairly fractionated in the chondrite-normalized diagram (Fig. 9a), with a flat light REE pattern and the lack of Eu anomaly (10.5 La; 2.2 Yb; chondrite-normalized La/Yb = 3.2). In the incompatible element-normalized diagram to the primitive mantle (PM), the pattern is gently sloped with K, Nb, and Ta weak enrichments, high Rb and Ba enrichments, and the lack of Ti anomaly (Fig. 9b). Geochemical features agree with a magma source of a continental tholeiite, but with the addition of K, Ba and Rb mobile lithophile elements. The weakly fractionated pattern with moderate contents of the most incompatible elements resulted from high degree of melting. However, the source was enriched in the more mobile lithophile elements by crustal fluids. The fluid addition lowers the solidus temperature and that may explain the high degree of melting.

The minettes of Croix-de-Vie and Payré (MIT and PMI) are intermediate rocks (52.6–57.0 wt% SiO_2; 5.0–5.7 wt% MgO) with a high Mg number of 70.6 to 73.2. They plot in the basaltic trachy-andesite and trachy-andesite fields (Fig. 8a). Titanium is low (0.8–1.2 wt% TiO_2). Alkali contents are high and dominated by K (1.5–3.0 wt% Na_2O;

Journal : Large 710	Article No : 786	Pages : 25	MS Code : 786	Dispatch : 1-7-2022

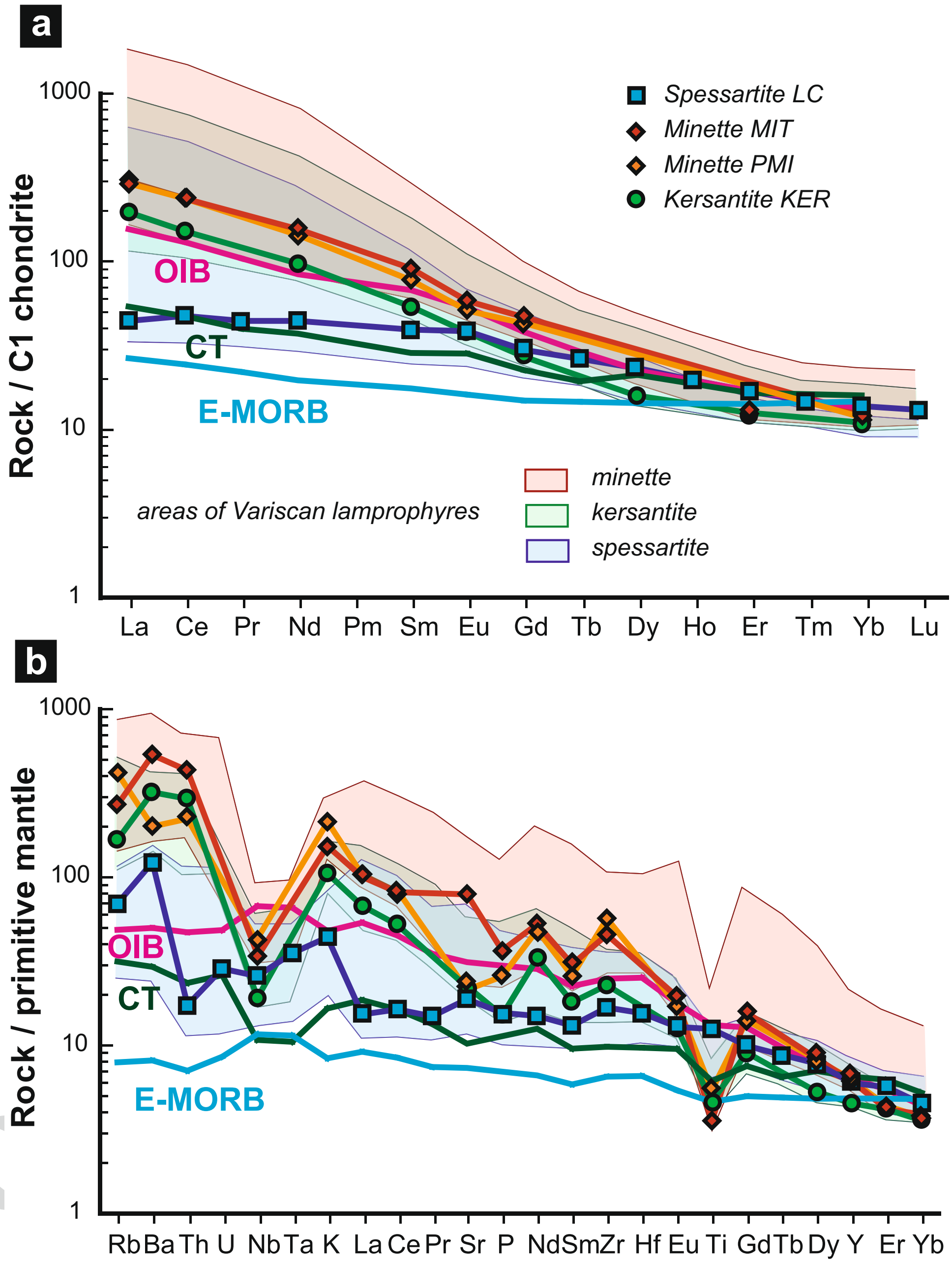

Fig. 9 **a** Trace element normalized patterns of the studied lamprophyres: C1 chondrite-normalized rare earth element diagram, normalization after McDonough and Sun (1995) E-MORB (enriched middle ocean ridge basalt), CT (continental tholeiite), and OIB (ocean island basalt) profiles are after Sun and McDonough (1989). **b** Trace element normalized patterns of the studied lamprophyres: Primitive mantle-normalized diagram, normalization after Sun and McDonough (1989). The spessartite displays patterns close to those of continental tholeiite (CT) except for enrichments of K, Ba and Rb. Minettes and the kersantite are highly fractionated in the lithophile and the more incompatible elements. They have important Nb- and Ti-negative anomalies. Kersantite is slightly depleted in the heavy rare earth elements. There are no Eu anomalies

4.6–6.5 wt% K_2O), the Payré minette being the more potassic (Fig. 8c). The norm composition is oversaturated. The high loss on ignition is partly due to the groundmass alteration, but also to the occurrence of primary carbonates. The compatible minor element contents are moderate (93–123 ppm V; 253–258 Cr; 20–21 Co; 133–153 Ni), and indicate that these rocks underwent a mild fractionation. Lithophile and the high field strength elements are high (171–265 Rb; 452–1675 Sr; 1404–3735 Ba; 19.0–36.7 Th; 27.9–28.3 Y; 510–636 Zr; 24.2–29.9 Nb). In the chondrite-normalized diagram (Fig. 9a), rare earth elements are fractionated with light rare earth enrichment and the lack of Eu-anomalies (69.2–71.1 La; 1.9 Yb; chondrite-normalized La/Yb = 24.5–26.1). In the incompatible element-normalized diagram to primitive mantle PM (Fig. 9b), patterns are steeply sloped with enrichments of the most incompatible and large ion lithophile element (LILE), but with important Nb- and Ti-negative anomalies.

The kersantite of l'Hôpital-Camfrout (KER) is an intermediate and magnesian rock (56.3 wt% SiO_2; 6.4 wt% MgO; Mg number = 69.8). It plots in the basaltic trachy-andesite to trachy-andesite fields (Fig. 8a). Titanium is low (1.0 wt% TiO_2). Alkali contents are moderate with similar Na and K values (3.2 wt% Na_2O; 3.2 wt% K_2O) (Fig. 8c). The norm composition is oversaturated. The loss on ignition is high

(4.9) due to the whole rock alteration. Compatible minor element contents are low to moderate (137 ppm V; 318 Cr; 14 Co; 68.6 Ni). Lithophile and the high field strength elements are moderate to high (106 Rb; 476 Sr; 2240 Ba; 24.9 Th; 20.6 Y; 256 Zr; 13.7 Nb). Rare earth elements are high and fractionated in the chondrite normalized diagram (Fig. 9a) with the lack of Eu-anomaly (46.5 La; 1.8 Yb; chondrite normalized La/Yb = 18). In the incompatible element diagram normalized to PM (Fig. 9b), the pattern is steeply sloped with LILE enrichment and Nb- and Ti-negative anomalies.

Discussion: late-to post-Variscan lamprophyres in Western Europe

Generalities

To perform the magmatic characteristics of the studied lamprophyres, as well as their geotectonic significance, we develop a comparison with a large set of Variscan lamprophyres dated from the Late Carboniferous to the Permian times. These intrusions were contemporaneous with syn- to post-collisional and late- to post-orogenic granites and associated magmatic formations. Lamprophyres are distributed in all the tectonic zones of the European Variscides from the western Armorican Massif to the easternmost Bohemian Massif and also in the Iberian Massif (Fig. 1). We do not consider the lamprophyres that have taken place outside the Variscan realm, such as the great swarms of Scotland and Scania.

French Armorican Massif

Lamprophyric dykes and sills are present in the whole Armorican Massif but were mainly investigated along the sea shores of the South-Armorican and North-Armorican zones.

The South-Armorican Zone is located at the south-west side of the suture of the South-Armorican and Centralian Variscan Ocean (Pouclet et al. 2017). In the Vendean area, sills of spessartite and dykes of minette are investigated in this study. At the westernmost end of the South-Armorican Zone (Cape Sizun of the Pointe du Raz, Finistère), a dyke of minette crosscuts the Late Carboniferous granite, but is yet undated (Cogné 1962).

In the Middle and Northern Armorican zones, lamprophyres are distributed in four areas. (1) In the Middle Western country of Daoulas, from the bay of Douarnenez to the Rade de Brest, the folded Devonian sedimentary strata are crosscut by a swarm of dykes and sills of kersantite. The studied kersantite of l'Hôpital-Camfrout (KER) was sampled in this area. As indicated above, these lodes are dated from Carboniferous to Early Permian (Caroff et al. 2021). (2) In the middle Brittany inland, around Châteaulin, Carhaix and Rostrenen, numerous small intrusions of minette, kersantite and rare spessartite are known but yet undated, because often highly altered. (3) In the northwestern Atlantic coast, near Plouarzel, a suite of dykes of minette are trending NNW-SSE and intrude the Aber Ildut granite dated at 303.8 ± 0.9 Ma by U–Pb method (Caroff et al. 2015). The minettes are dated at 272.5 ± 13.7 Ma by K–Ar method (Bellon et al. 1988). (4) In the north coast of Brittany, some dykes of minette are hosted by the Late Carboniferous granite of Ploumanac'h. Lastly, the northern seashore of Cotentin in Normandy and the coast of the Channel Islands of Jersey and Guernsey exhibit numerous dykes and sills of minette and kersantite cross-cutting granite massifs and Devono-Carboniferous metasediments (Le Gall et al. 1989). A dyke of Guernsey has been dated at 295 ± 8 Ma by K–Ar method (Adams 1976). The lamprophyres coexisted with a volcanic activity of K-rich olivine basalts.

Chemical analyses of major and minor elements of lamprophyres of the Armorican Massif are available from Turpin et al. (1988), Bellon et al. (1988), Chauris and Hallégouët (1994), and Caroff et al. (2015, 2021).

English Cornwall

In the Cornwall region, SW England peninsula, lamprophyre dykes intruded Devonian to Carboniferous volcano-sedimentary formations of the Avalonian terrane. They consist mainly of minettes with subordinate kersantites. On the basis of Ar–Ar geochronological data, dykes are dated between 293.6 and 285.4 Ma in the Early Permian (Dupuis et al. 2015). Their emplacement was coeval with the post-collisional Cornubian granite batholith. Previous data also indicated contemporary basaltic lava activities with the lamprophyre intrusions around 291 ± 6 Ma (recalculated K–Ar analyses from Thorpe et al. 1986).

French Massif Central

In the French Massif Central, all the granite plutons are crosscut by numerous late-magmatic dykes and veins of micrograined rocks with a wide range of acidic to mafic compositions. Mica-rich rocks displaying lamprophyric textures are often described as vaugnerites, though some of them have be termed minettes. True vaugnerites are biotite enriched monzodiorites embedded in granite plutons, migmatites or schists. Vaugnerites are dated between 336 and 299 Ma (Laurent et al. 2017). Conversely, numerous dykes of post-orogenic Variscan lamprophyres, mainly minettes and kersantites, are pointed out in regional studies. However, very few have been analysed and dated.

Minette dykes trending NNE-SSW intruded the Late Carboniferous leucogranite of St-Sylvestre in the Limousin western part of the Massif Central (Chalier and Sabourdy 1987). One sample was dated at 295 ± 10 Ma by Rb–Sr method (Leroy and Sonet 1976). It was analysed by Turpin et al. (1988). In a neighbouring area, the St-Yriex gold district, minette dykes crosscut the Lower Allochthon Gneiss and one sample is dated at 290 ± 5 Ma by Rb–Sr method (Chalier et al. 1994). At the westernmost side of Massif Central, in the Charroux-Civray pluton Complex, dykes of lamprophyres have been crossed in two drill holes (Cuney et al. 2001) but not studied.

At the middle-eastern side of the Massif Central, lamprophyre dykes crosscut the granite of Monts du Forez. They consist mainly of kersantites and secondary of spessartites (Jeambrun et al. 1976). One kersantite has been dated at 316 ± 20 Ma by Rb–Sr method (Cantagrel et al. 1970). To the northeast, numerous dykes of kersantite and minette are located in the Morvan Massif. They intruded the granite, but also the Visean and Stephanian volcano-sedimentary formations (Carrat et al. 1986; Delfour et al. 1997). One kersantite has been dated at 301 Ma by Rb–Sr method (Cuney and Sonet, unpublished). One minette has been analysed by Turpin et al. (1988).

To the southeast of Massif Central, dykes of lamprophyres trending N-S intruded the schist of the Cévennes Massif of Lozère (Brouder et al. 1977; Faure et al. 2009). Most of these rocks have mineral composition of kersantite, though some biotite-rich thin dykes can be termed minette. Their genetic relationships with the Late Carboniferous granites of Aigoual and Mont Lozère are unknown. One dyke has been dated at 286 ± 3 Ma by zircon U–Pb method (Faure et al. 2009).

South of the Massif Central, a dyke of minette crosscuts Devonian limestones of the Mouthoumet Massif. It has been analysed and dated at 319 ± 5 Ma by Ar–Ar (Durand-Delga et al. 1997).

Moreover, to the south of the Parisian Basin, at Couy, a borehole has been drilled in the crystalline basement in the continuation of the Massif Central formations below the basin. Several lodes of lamprophyres have been crossed (Wagner et al. 1992). A sample of minette has been analysed and dated at 301.5 ± 6.2 Ma by Ar–Ar method with biotite (Costa 1990). Another minette has been dated around 292 Ma by K–Ar method (Hottin and Calvez 1988). Above the gneiss basement, the bottom of the sedimentary pile consists of Stephanian sediments and interbedded mafic lavas of high K trachy-andesite composition similar to the minette composition (Hottin et al. 1992). Ar–Ar analysis on biotite yields a plateau age of 301.6 ± 6.3 Ma (Costa and Maluski 1988). It is concluded that the volcanic activity took place at the Stephano-Autunian time (Gzhelian) and that dykes of minettes have fed the lava flows.

French South Vosges and German Schwarzwald (Black Forest)

The Vosges Massif is divided in two parts, South Vosges and North-Vosges, by the Lalaye-Lubine/Baden Baden shear zone, an ophiolitic suture between the Moldanubian Zone to the south and the Saxo-Thuringian Zone to the north. The Schwarzwald matches with the South-Vosges in the same tectonic zone, in being separated by the Cenozoic rift or the Upper Rhine Graben. Both regions betray similar late to post-orogenic potassic and ultrapotassic magmatism with, first, intrusive bodies of vaugnerites or durbachites dated around 340–335 Ma (Guillot et al. 2020), similar to vaugnerites of the Massif Central, and second, dyke swarms of lamprophyres mainly consisting of minettes and kersantites.

Lamprophyres have intruded low-grade sedimentary and volcanic formations of Early Palaeozoic, medium- to high-grade gneiss complexes and granitoids dated at the Early Carboniferous, and post-collisional (after 340 Ma) granites dated at Late Visean. In Schwarzwald, four dykes have been dated between 332 and 314 Ma by Ar–Ar method (Bashkirian) (Hegner et al. 1998). Plateau ages give 332 ± 2, 330 ± 2, 325 ± 2, and 314 ± 2 Ma. However, many other dykes may be younger (Soder and Romer 2018). The oldest lamprophyre dykes were contemporaneous with rhyodacite dykes related to coeval undeformed granitoids, and thus with melting of the crust. According to Hegner et al. (1998) "They have witnessed the post-collisional development of the orogeny because they post-date peak metamorphism and were emplaced during transtensional tectonics".

Chemical analyses are done by Turpin et al. (1988), Hegner et al. (1998) and Soder (2017). Soder (2017) has analysed more than one hundred of lamprophyre dyke rocks from Vosges, Schwarzwald, Odernwald and Spessart. We retain the analyses selected by Soder and Romer (2018).

French North Vosges, German Odenwald and Spessart

North Vosges, Odenwald and Spessart locate in the Saxo-Thuringian Zone and its basement wedge, the Mid-German Crystalline Zone. Lamprophyres intruded metasedimentary and volcano-sedimentary formations in North-Vosges, and high-grade metamorphic rocks and Carboniferous granites in North Vosges, Odenwald and Spessart. The lamprophyre types consist of minettes, kersantites and spessartites-vogesites, the latter being more common in Spessart. In Vosges, spessartites are not discriminated to vogesites in the lack of feldspar distinction. Some minettes display peralkaline compositions close to lamproites (high K_2O and light rare earth element contents).

Spessartites from Odenwald and Spessart have been dated by Ar–Ar method from late Visean to Serpukhovian

(334 ± 4; 329 ± 2; 324 ± 1 Ma) (von Seckendorff et al. 2004). Chemical analyses are done by Turpin et al. (1988), von Seckendorff et al. (2004), Soder (2017), and Soder and Romer (2018).

Bohemian Massif

The Bohemian Massif is divided in three parts by the Teplá Fault, a NE-SW trending suture, and by the Elbe lineament, a major NW–SE fault parallel to the Erzegebirge fault system: 1) the Teplá-Barrandian and Moldanubian units of the Moldanubian tectonic Zone at the middle and southeastern part, 2) the Erzgebirge part the Saxo-Turingian Zone to the north, and 3) the Sudetes part to the east with the central Sudetes, the west Sudetes and Lusatian region, both attributed to the Saxo-Turingian Zone, and the south-easternmost Sudetes that is the Moravo-Silesian terrane assigned to the Rheno-Hercynian Zone. Syn- to post-orogenic ultra-potassic bodies have intruded the whole massif (Krmíček 2010).

In the Moldanubian Zone, intrusions are related to two diachronous pulses: a late syn-tectonic durbachite series around 342–339 Ma and a post-tectonic suite of syenitoids and lamprophyres around 336–335 Ma with a long temporal range of lamprophyric magmatic activity from 334 to 274 Ma (Janoušek et al. 2010; Krmíček 2010; Krmíček et al. 2020a). Lamprophyres display various compositions of spessartites, minettes and kersantites. They are associated with minor lamproites (Krmíček 2010). In the Prague Basin, minettes and kersantites crosscut the sedimentary sequences of the Teplá-Barrandian Unit. In the middle Moldanubian Zone, dyke swarms of minettes and kersantites intruded the Variscan granitoids of the Iron Mountains between Prague and Brno (Krmíček et al. 2014). In the southern region, dykes of kersantites and spessartites intruded the South Bohemian Batholith. They are dated from 334 to 318 Ma by Rb–Sr method (Neubauer et al. 2003; Zeitlhofer et al. 2016). Representative chemical analyses are given by Krmíček et al. (2014) and by Zeitlhofer et al. (2016).

The Erzgebirge is the main part of the northwestern part of the Bohemian Massif in the Saxo-Thuringian Zone at the Germany-Czech Republic boundary. This region is an important ore deposit province with a long-standing mining history. Numerous dyke swarms of lamprophyres intruded the core complex gneisses, late-collisional granites and low-grade meta-sediments according to fault systems trending NW–SE and SW-NE. They are coeval with ultrapotassic mafic volcanics. Numerous ages performed by K–Ar, Ar–Ar, and zircon U–Pb methods are available from Kurze et al. (1998), Werner and Lippolt (1998), von Seckendorff et al. (2004) and Seifert (2008). A thorough study of metallogeny and petrogenesis of lamprophyres is available from Seifert (2008). This author divided the Erzgebirge lamprophyres in three main groups (LD1, 2 and 3) using criteria of petrography and geochemistry, and relatively age relationships to late-Variscan volcano-plutonic activity and mineralization phases. The LD1 late-collisional group includes kersantites and spessartites that predate all the epigenetic mineralization events. It is dated between 335 and 325 Ma. The LD2 post-collisional group is dominated by minettes and kersantites that are related to polymetallic mineralization events but predated the Sn- and Ag-base metal ore bodies. It is dated between 325 and 290 Ma. The LD3 post-collisional group mainly consists of feldsparphyric kersantites post-dating the Sn-polymetallic mineralization but predating the Ag-base metal ores. It is dated between 315 and 290 Ma and is contemporaneous with rhyolitic intrusions. Abundant analytical data are done by von Seckendorff et al. (2004), Seifert (2008), and Štemprok et al. (2014).

Sudetes and Lusatia areas are located in the Elbe Zone at the north-eastern margin of the Bohemian Massif. This zone is separated from the Central Bohemian Massif by the NW–SE Elbe lineament. The whole Sudetes region is intruded by dyke swarms of lamprophyres with about 150 veins of spessartites-vogesites, minettes and kersantites (Awdankiewicz 2007). There are also some dykes of lamproites (Krmíček et al. 2020b). These intrusions have occurred during a wide age range of 330–296 Ma. For example, a spessartite has been dated at 333.1 ± 3.1 Ma and a minette at 312 ± 4 by U–Pb method; a kersantite has been dated at 324 ± 3 Ma and a minette at 314 ± 6 by Ar–Ar method (von Seckendorff et al. 2004; Awdankiewicz 2007; Mikulski and Williams 2010a and b). At Lusatia, lamprophyre dykes mainly consist of spessartites (Abdelfadil 2013). They have been dated between 335 and 325 Ma and can be correlated with the LD1 late-collisional lamprophyre group of the Erzgebirge. Trace element chemical analyses are available from von Seckendorff et al. (2004), Awdankiewicz (2007), and Abdelfadil (2013).

Variscan Alp

Lamprophyres are found in metamorphic formations of Alpine domains in the Variscan basement of the External Crystalline Massifs and of the Western Alps.

At the Gothard Massif, dismembered lamprophyre dykes have been discovered in blocks of gneiss embedded in a calcschist formation. They are spessartites and kersantites dated from 291 to 285 Ma by U–Pb method (Bussien et al. 2008). At the Austroalpine Dent Blanche nappe, dykes of camptonites crosscut a Permian layered mafic complex. A sample has been dated at 260.2 ± 0.7 Ma by Ar–Ar method (Monjoie et al. 2007). At the Argentera Massif, swarms of spessartites have intruded into Variscan migmatites and early Permian granitoids (Filippi et al. 2019). It is not possible to decipher for the initial tectonic zone setting of these intrusions in the Variscan realm. However, age dating allows for assigning these rocks to the late- to post-Variscan magmatic activities.

Iberian Massif

At the Central Iberian Zone of the Iberian Massif, unless than nine dyke swarms of mafic alkaline lamprophyres have intruded the Variscan Spanish Central System of synorogenic to late orogenic granitoids. The dyke rocks consist of camptonites with a few evolved bostonites. They have been dated between 283 and 264 Ma and are thus related to the late- and post-orogenic geodynamic evolution (Bea et al. 1999; Orejana et al. 2008; Scarrow et al. 2006, 2011). At the Southern Iberian Massif, dykes of kersantite crosscut a monzogranite pluton dated ca. 314–304 Ma (Errandonea-Martin et al. 2018). The pluton enclosed dioritoid bodies of vaugnerite having a composition similar to that of the calc-alkaline lamprophyres with mixing/mingling textures giving evidence of syn-plutonic embedding of the vaugneritic bodies. It is expected that the lamprophyres emplaced just after the pluton setting. Representative analyses are given by Orejana et al. (2008), Scarrow et al. (2011) and Errandonea-Martin et al. (2018).

Geochemical features of the Variscan lamprophyres

Covariation diagrams display a broad spectrum of chemical compositions of lamprophyres in terms of high field strength and large ion lithophile elements (HFSE and LILE). It is shown first with the La/Yb versus La diagram (Fig. 10). The La/Yb ratio ranges from 5 to 95 with increasing values from spessartites to kersantites and minettes. The ratio values depend either on the La or the Yb enrichments. There are poor correlations of La with Yb, Th, Ba, Nb, Zr, Sr, Rb, and Ti, representative HFS and LIL elements, which display large range of contents (Fig. 11). These features are the result of variable degree of melting from different sources and contaminations by crust melts and fluids. The La Chaume spessartite shares similar composition with the La-poor spessartites of Lusatia, except for its high Ba content. The Vendean minettes and the Brittany kersantite display average compositions of the calc-alkaline Variscan lamprophyres. A distinct magmatic source matches the alkaline lamprophyres namely the camptonites of the Central Iberian Zone that plot in areas rich in Nb and Ti, but poor in Th. A singular geochemical composition is also shown by the lamprophyres group LD3 of Soder (2008) from Erzgebirge with AQ2 higher Yb and Ti, and lower Th and Sr contents compared with the averaged calc-alkaline lamprophyres.

Mantle sources and subduction-related signals may be indicated in the Th/Yb versus Nb/Yb diagram after Pearce (2008) in Fig. 12a. This diagram suggests that most of the lamprophyres were generated by melting of metasomatically enriched mantle including assimilation and fractional crystallization (AFC) processes. The original mantle sources can be search in the MORB-OIB array. The Spanish camptonites plot in the mantle source array close to OIB. Unlike to the calc-alkaline lamprophyres, these alkaline lamprophyres

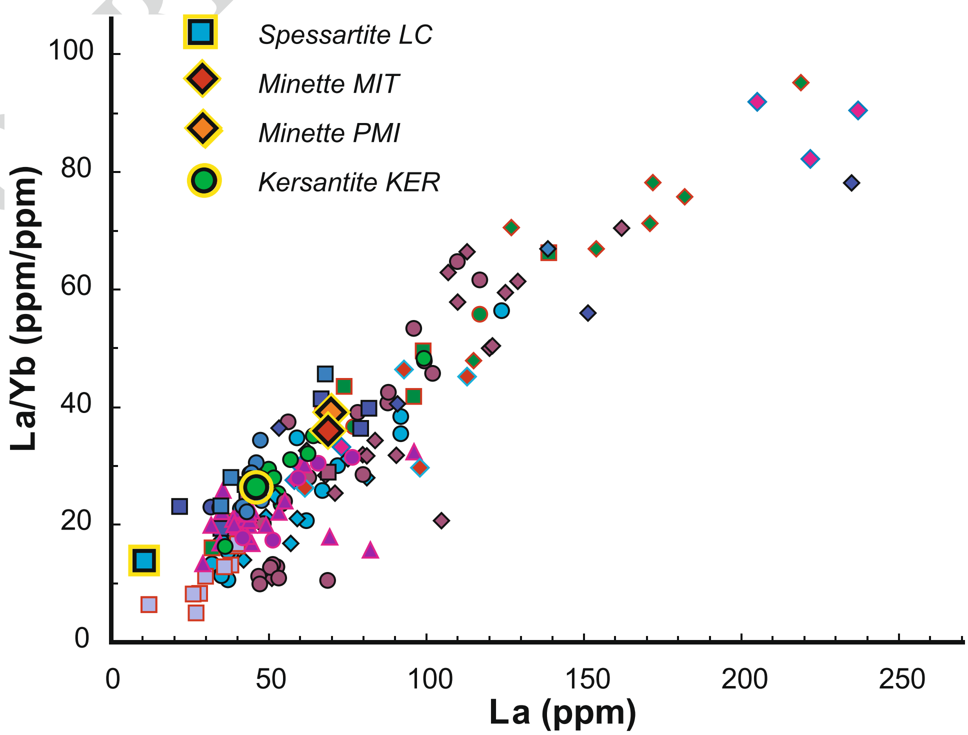

Fig. 10 La/Yb versus La diagram (ppm values). Same symbols as for Fig. 8. The La/Yb ratio ranges from 5 to 95 with increasing values from spessartites to kersantites and minettes

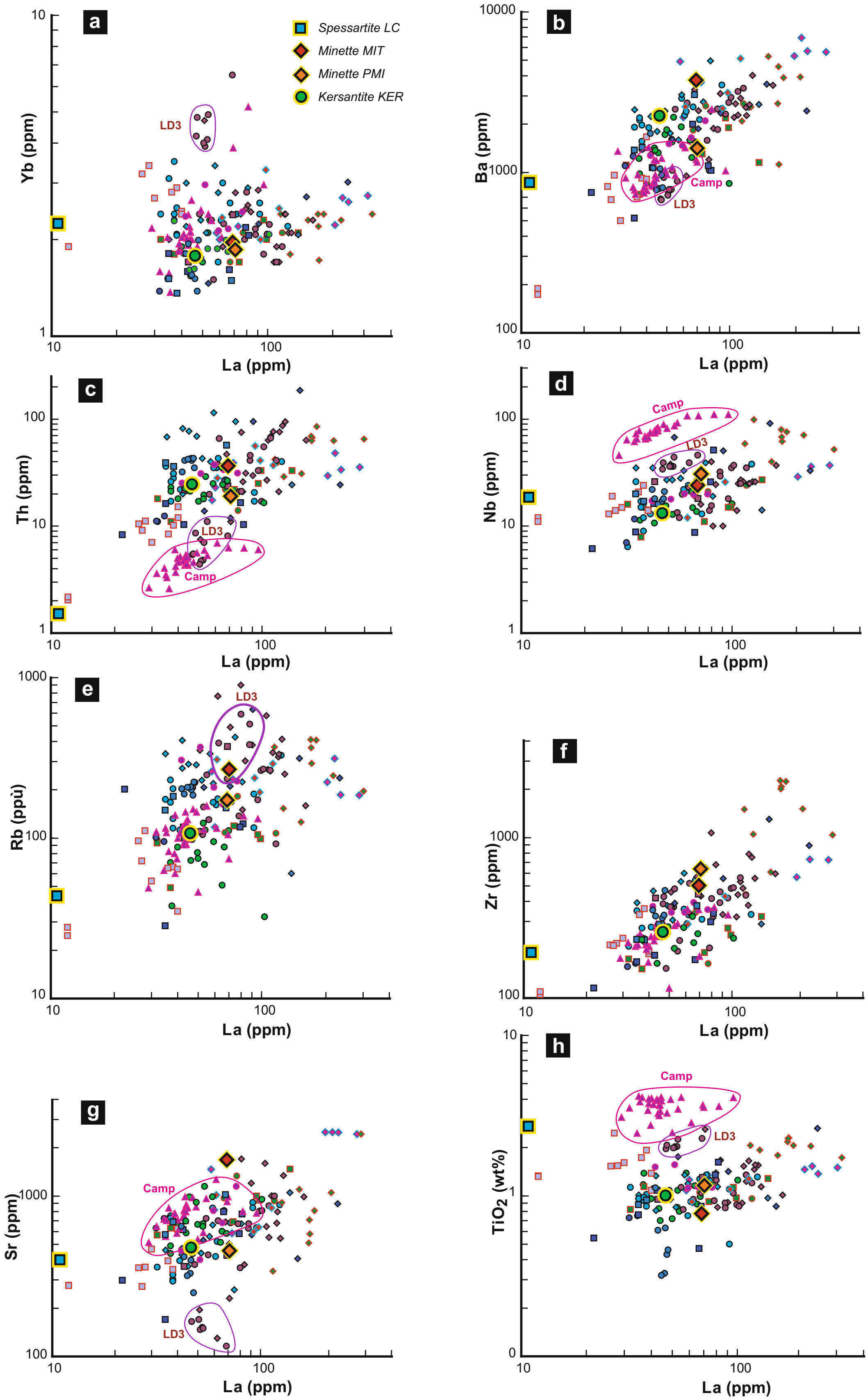

Journal : Large 710	Article No : 786	Pages : 25	MS Code : 786	Dispatch : 1-7-2022

◂**Fig. 11** **a–h** Bivariate diagrams of selected trace elements, Yb, Ba, Th, Nb, Rb, Zr, Sr, and TiO_2 versus La (ppm values except wt% for TiO_2). Analytical set of Fig. 8. The spreading of the element contents provides evidence of the involvement of a number of sources of magma, which have underwent different contaminations, degrees of melting and differentiation process. Distinct sources are displayed for the Spanish camptonites (Camp) and post-orogenic lamprophyres of Erzgebirge (LD3). Crustal contributions are shown by Th, Ba, and Rb enrichments. Poor positive correlation trends can be related to assimilation and fractional crystallisation (AFC) processes

did not generate in a contaminated mantle but in an asthenospheric enriched mantle (Bea et al. 1999). Similarly, the source of the post-orogenic LD3 lamprophyres of Erzgebirge was involved in a post-orogenic asthenospheric upwelling.

Mantle metasomatism may take place during different events such as subduction and continental collision, which have occurred during the Variscan orogeny. These events commonly caused crustal contamination of the mantle by ocean sediments or continental formations with the addition of crustal melts and fluids. The addition of fluids mainly occurs during subduction of altered ocean crust and sediments with flux-melting of the mantle wedge. In return, continental subduction more likely implies dehydrated lithologies. However, the breakdown of high pressure hydrous phases created during metasomatic processes may initiate melting during late orogenic regional extension with decompression and heating (Foley 1992). Contributions from the continental crust, altered oceanic crust and sediments are

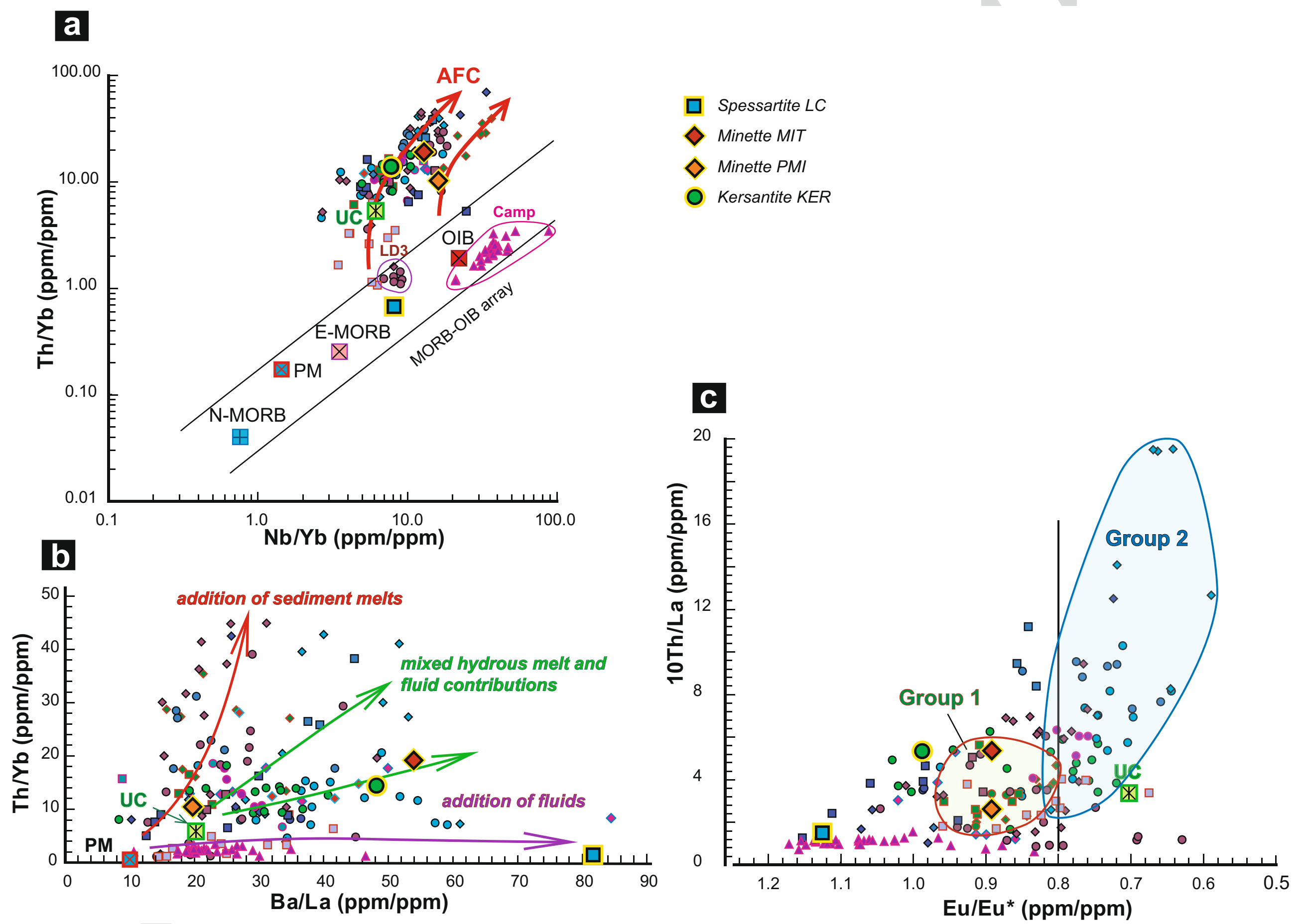

Fig. 12 **a** Th/Yb versus Nb/Yb diagram after Pearce (2008) (ppm values). Analytical set of Fig. 8. PM (primitive mantle), N-MORB, E-MORB and OIB after Sun and McDonough (1989). UC, upper crust after Rudnick and Gao (2004). AFC, assimilation and fractional crystallisation process. LD3, post-collisional lamprophyres of Erzgebirge (Seifert 2008). Camp, camptonites of the Central Iberian Zone (Orejana et al. 2008; Scarrow et al. 2011; Errandonea-Martin et al. 2018). The calc-alkaline lamprophyre magma source could be the fairly enriched lithospheric mantle contaminated during subduction and collision events and evolved by AFC processes. **b** Ba/La versus Th/Yb versus Ba/la diagram after Woodhead et al. (2001) (ppm values). Contamination of the mantle sources may result from two distinct and possibly associated processes: addition of fluids from subducted slabs with main enrichment in Ba and addition of hydrous melts from oceanic and/or continental rocks with main enrichment in Th. **c** 10Th/La versus Eu/Eu* diagram after Soder and Romer (2018) (Th and La, ppm values; Eu and Eu* = $\sqrt{Sm}$ x $\sqrt{Gd}$, chondrite-normalized values after McDonough and Sun 1995). Group 1, lamprophyres of North Vosges, Odenwald and Spessart of the Saxo-Thuringian Zone. Group 2, lamprophyres of South Vosges and Schwarzwald of the Moldanubian Zone. The Armorican lamprophyres belong to Group 1

Journal : **Large 710**	Article No : **786**	Pages : **25**	MS Code : **786**	Dispatch : **1-7-2022**

indicated by enrichments of the lithophile elements and peculiarly the more mobile ones by the addition of fluids. Contamination processes by crustal melt or fluids can be discriminated according to variable increasing contents of Th, Ba or Rb. The moderately mobile light rare earth elements are variably modified. Th enrichment is provided by crust melt while Ba is transported by fluids. Consequently, the Th/Yb versus Ba/La diagram of Woodhead et al. (2001) is used to discriminate the contributions of hydrous melts and fluids. In this diagram, Fig. 12b, the calc-alkaline lamprophyres display mixed processes of mantle contamination with either assimilation of sediments melts or of fluids in varied proportions. The Vendean minettes and Brittany kersantite sources were mainly enriched in fluids with moderate contributions of sediment melts. In return, the La Chaume spessartite source is only concerned by the addition of fluids.

Distinct metasomatized magmatic sources from different processes of mantle enrichment have been advocated for Variscan lamprophyres. In SW Germany and easternmost France, Soder (2017) and Soder and Romer (2018) have distinguished two groups of lamprophyres. Group 1 locates in North Vosges, Odenwald and Spessart. Lamprophyres belong to the Mid-German Crystalline and Saxo-Thuringian zones and comprise abundant amphibole lamprophyres. Their sources are mainly concerned by the addition of sediments melts due to continental subduction and collision. Group 2 locates in South Vosges and Schwarzwald. Lamprophyres belong to the Moldanubian Zone and predominantly consist of mica lamprophyres. Their source implies mixed hydrous melt and fluid contributions from altered oceanic crust and sediments related to ocean subduction. Incompatible element ratios and Sr–Nd-Pb isotopic compositions have revealed two distinct crust-derived metasomatic signatures, which are indicative for mantle enrichment during different stages of subduction of ocean and/or continental materials. Geochemical differences concern a flattener LILE pattern of Group 2 with clear negative Eu-anomalies. Fractionated LILE resulted in high Th/La ratios. Hence, the group distinction is shown in the Th/La versus Eu/Eu* diagram of Soder (2017). In Fig. 12c, we plot the analyses of Groups 1 and 2 selected by Soder and Romer (2018) with analyses from a dataset of Variscan lamprophyres. The two groups are broadly discriminated by the Eu/Eu* value of 0.8. Lamprophyres of Group 1 are recognized in many parts of the Saxo-Thuringian Zone where a wide range of rocks have subducted and collided during the closure of the Rheic Ocean. In the high-grade gneiss, relict granulite, eclogite and garnet-peridotite indicate that continental crust was subducted to mantle depths during the Variscan collision between the Moldanubian and Saxo-Thuringian zones (Schaltegger et al. 1996; Skrzypek et al. 2012; Tabaud et al. 2014). Lamprophyres of Group 2 are recognized in the Moldanubian Zone of the Bohemian Massif, which underwent a HP metamorphism with mantle metasomatism around 340 Ma (Schaltegger et al. 1996). Their negative Eu-anomalies attest for the input of evolved crustal formations in metasomatized sources.

The South Armorican lamprophyres share geochemical features with Group 1 lamprophyres of the Saxo-Thuringian Zone. Their sources were metasomatized during a convergent event of subduction and continental collision, which involved the South Armorican Ocean. However, the contamination components of the sources are dominated by addition of fluids with secondary contribution of crustal melts (Fig. 12b). These characteristics imply a geotectonic context of ocean subduction with limited involvement of continental collision.

Conclusions

Investigations of some new sites of lamprophyres in the South Armorican Zone are the matter to document late to post-orogenic magmatic activities of the Variscan belt. In the Vendean area, spessartite sill intrusion was coeval with the setting of a Carboniferous late-orogenic granite dated around 320 Ma. Dykes of minette are correlated with the post-orogenic Early Permian tectonic activity, one dyke being dated at 286.2 ± 6.6 Ma. The West Brittany kersantite swarm intruded the Late Devonian folded sedimentary sequences. It is dated to the Middle Carboniferous.

Geochemical features of the Variscan lamprophyres are commonly used to trace the nature of the deeply subducted materials, which contaminated the mantle sources. The calc-alkaline lamprophyres of the tectonic zones of the Variscan Belt display different compositions in term of minor or major involvements of subduction materials from subducted oceanic or continental crusts and from collided and deeply buried continental margins. Though limited in number, the analyses of the Armorican lamprophyres allow the determination of their magma genesis. Spessartite originated from high degree of melting of a lithospheric mantle enriched in mobile lithophile elements possibly by subducted slab fluids. Intrusion of the spessartite sills has occurred during the middle to late Carboniferous anatectic event linked to the crustal thickening. Minettes and kersantites originated from melting of a lithospheric mantle metasomatized by fluids and melts derived from subducted oceanic crust with minor contribution of continental crust. The fluid addition was more important for the minettes. Their dykes were emplaced during the Early Permian post-collisional extension. It is suspected that their magma sources were contaminated as a result of the closure of the South Armorican Ocean by subduction and continental margin collision. AQ3

Journal : Large 710	Article No : 786	Pages : 25	MS Code : 786	Dispatch : 1-7-2022

Acknowledgements The minerals were analysed in the Service Camparis of the University of Paris-Sorbonne, Paris (France). The minette of Croix-de-Vie has been dated at the Geochronological laboratory of the University of Brest, Laboratoire Géosciences Océan, Institut Universitaire Européen de la Mer (France). The analysis of the spessartite LC was done at the Centre de Recherches Pétrographiques et Géochimiques (CRPG) of Nancy (France). The minettes MIT, PMI, and the kersantite KER have been analysed at the Analytical laboratory of the University of Brest, Institut Universitaire Européen de la Mer (France). We thank Céline Liorzou for the chemical analyses of the minettes and the kersantite. We are grateful to two anonymous reviewers for conspicuous critics and constructive comments for improving the first version of the text.

References

Abdelfadil KM (2013) Geochemistry of Variscan lamprophyre magmatism in the Saxo-Thuringian Zone. PhD thesis, Univ Potsdam, p X+108

Adams CJD (1976) Geochronology of the Channel Islands and adjacent French mainland. J Geol Soc London 132:233–250

Awdankiewicz M (2007) Late Palaeozoic lamprophyres and associated mafic subvolcanic rocks of the Sudetes (SW Poland): petrology, geochemistry and petrogenesis. Geol Sudetica 39:11–97

Ballèvre M, Bosse V, Ducassou C, Pitra P (2009) Palaeozoic history of the Armorican Massif: models for the tectonic evolution of the suture zones. CR Geosci Paris 341:174–201

Bayliss P (1975) Nomenclature of the trioctaedral chlorites. Can Mineral 13:178–180

Bea F, Montero P, Molina JF (1999) Mafic precursors, peraluminous granitoids, and late lamprophyres in the Avila batholith: a model for the generation of Variscan batholiths in Iberia. J Geology 107:399–419

Bellon H, Chauris L, Hallégouët B, Thonon P (1988) Magmatisme fissural permien et triasique dans le Pays de Léon (Massif armoricain, France). CR Acad Sci Paris 307 sér 2:2049–2054

Bellon H, Rangin C (1991) Geochemistry and isotopic dating of Cenozoic volcanic arc sequences around the Celebes and Sulu Seas. In: Silver E, Rangin C (eds) Proceedings of the Ocean Drilling Program Texas, USA, Scientific Results, Vol 124, pp 51–63

Brouder P, Gèze B, Macquar JC, Paloc H (1977) Notice explicative, Carte géol France (1/50 000), feuille Meyrueis (910). Bureau Rech Géol Minières, Orléans, p 29

Bussien D, Bussy F, Masson H, Magna T, Rodionov N (2008) Variscan lamprophyres in the Lower Penninic domain (Central Alps): age and tectonic significance. Bull Soc Géol Fr 179(4):369–381

Cantagrel JM, Valizadeh MV, Vialette Y (1970) Âge des granites, granophyres et kersantites de la région de Thiers (Puy-de-Dôme). CR Acad Sci Paris Sér D 270:600–603

Carignan J, Hild P, Mevelle G, Morel J, Yeghicheyan D (2001) Routine analyses of trace elements in geological samples using flow injection and low pressure on-line liquid chromatography coupled to ICP-MS: a study of reference materials BR, DR-N, UB-N, AN-G and GH Geostandard Newsletter. J. Geostandards Geoanalysis 25(2–3):187–198

Caroff M, Labry C, Le Gall B, Authemayou C, Bussien Grosjean D, Guillong M (2015) Petrogenesis of Late-Variscan high-K alkali-calcic granitoids and calc-alkaline lamprophyres: The Aber-Ildut/North-Ouessant complex, Armorican Massif, France. Lithos 238:140–155

Caroff M, Barrat JA, Le Gall B (2021) Kersantites and associated intrusives from the type locality (Kersanton), Variscan Belt of Western Armorica (France). Gondwana Res 98:45–62

Carrat H, Lefavrais-Raymond A, Sambier A (1986) Notice explicative, Carte géol. France (1/50 000), feuille Château-Chinon (523). Bureau Rech Géol Minières, Orléans, p 87

Chalier M, Sabourdy G (1987) Les lamprophyres du granite hyperalumineux de Saint-Sylvestre (Limousin, Massif Central français). Caractères pétrologiques et origine. CR Acad Sci Paris 305 sér 2:99–105

Chalier M, Virlogeux D, Duthou JL (1994) Les lamprophyres du district aurifère de Saint-Yriex (Limousin, Massif Central français). Âge Rb/Sr Autunien et relations chronologiques avec le dépôt de l'or. CR Acad Sci Paris 319 sér 2:1511–1518

Chauris L, Hallégouët B (1994) Notice explicative de la feuille Plouarzel-Île d'Ouessant (237). Orléans, Bureau Rech Géol Minières, p 11

Cogné J (1962) La sizunite (Cap Sizun, Finistère) et le problème de l'origine des lamprophyres. Bull Soc géol France S7-IV:141–156

Costa S (1990) De la collision continentale à l'extension tardi-orogénique : 100 millions d'années d'histoire varisque dans le Massif Central français. Une étude chronologique par la méthode 40Ar-39Ar. PhD thesis, Univ Montpellier 2, p 441

Costa S, Maluski H (1988) Datations par la méthode 39Ar-40Ar de matériel magmatique et métamorphique paléozoïque provenant du forage de Couy-Sancerre (Cher, France). Programme G.P.F. CR Acad Sci Paris 306 sér 2:351–356

Cotten J, Le Dez A, Bau M, Caroff M, Maury R, Fourcade S, Bohn M, Brousse R (1995) Origin of rare-earth element and yttrium enrichments in subaerial exposed basalts: evidence from French Polynesia. Chem Geol 119:115–138

Cox A, Dalrymple GB (1967) Statistical analysis of geomagnetic reversal data and the precision of potassium-argon dating. J Geophys Res 72:2603–2614

Cuney M, Brouand M, Stussi JM, Virlogeux D (2001) Le complexe plutonique de Charroux-Civray (Vienne): témoin du magmatisme infra-carbonifère dans le segment occidental de la chaîne varisque européenne. Géol Fr 1–2:143–166

Delfour J, Alabouvette B, Cornet J (1997) Notice explicative, Carte géol. France (1/50 000), feuille Corbigny (496). Bureau Rech Géol Minières, Orléans, p 93

Dupuis N, Braid JA, Murphy JB, Shail RK, Archibald DA, Nance RD (2015) 40Ar/39Ar phlogopite geochronology of lamprophyre dykes in Cornwall, UK: new age constraints on Early Permian post-collisional magmatism in the Rhenohercynian Zone, SW England. J Geol Soc London 172:566–575

Durand-Delga M, Montigny R, Rossi P (1997) Âge namurien du lamprophyre de Termes (massif de Mouthoumet, Aude): sa signification dans l'édifice varisque pyrénéen. Géol Fr 3:13–20

Erdmann S, Martel C, Pichavant M, Kushnir ARL (2014) Amphibole as an archivist of magmatic crystallization conditions: problems, potential, and implications for inferring magma storage prior to the paroxysmal 2010 eruption of Mount Merapi. Indonesia Contrib Mineral Petrol 167:1016. https://doi.org/10.1007/s00410-014-1016-4

Errandonea-Martin J, Sarrionandia F, Carracedo-Sánchez M, Gil Ibarguchi JI, Eguíluz L (2018) Petrography and geochemistry of late- to post-Variscan vaugnerite series rocks and calc-alkaline lamprophyres within a cordierite-bearing monzogranite (the Sierra Bermeja Pluton, southern Iberian Massif. Geol Acta 16(3):237–255

Faure M, Brouder P, Thierry J, Alabouvette B, Cocherie A, Bouchot V (2009) Notice explicative, Carte géol. France (1/50 000), feuille Saint-André-de-Valborgne (911). Bureau Rech Géol Minières, Orléans, p 138

Filippi M, Zanoni D, Gosso G, Lardeaux J-M, Verati C, Spalla MI (2019) Structure of lamprophyres: a discriminant marker for Variscan and Alpine tectonics in the Argentera-Mercantour Massif. Maritime Alps Earth Sci Bull 190:12

Foley S (1992) Vein-plus-wall-rock melting mechanisms in the lithosphere and the origin of potassic alkaline magmas. Lithos 28:435–453

Guillot F, Averbuch O, Dubois M, Durand C, Lanari P, Gauthier A (2020) Zircon age of vaugnerite intrusives from the Central and Southern Vosges crystalline massif (E France): contribution to the geodynamics of the European Variscan belt. Earth Sci Bull 191:26–55

Hawthorne FC, Oberti R, Harlow GE, Maresch WV, Martin RF, Schumacher JC, Welsch MD (2012) Nomenclature of the amphibole supergroup. Am Min 97:2031–2048

Hegner E, Kölbl-Ebert M, Loeschke J (1998) Post-collisional Variscan lamprophyres (Black Forest, Germany): $^{40}Ar/^{39}Ar$ phlogopite dating, Nd, Pb, Sr isotope, and trace element characteristics. Lithos 45:395–411

Hey MH (1954) A new review of the chlorites. Mineral Mag 30:277–292

Hottin AM, Calvez JY (1988) Résultats analytiques K-Ar et Rb-Sr sur quelques minéraux du forage de Sancerre-Couy. Bureau Rech Géol Minières, Orléans, Document 137:225–234

Hottin AM, Marteau P, Turland M (1992) Comparaisons entre les roches volcaniques du forage de Sancerre-Couy et celles des bassins stéphaniens du nord-ouest du Massif central. Géol Fr 3–4:37–42

Janoušek V, Holub FV, Magna T, Erban V (2010) Isotopic constraints on the petrogenesis of the Variscan ultrapotassic magmas from the Moldanubian Zone of the Bohemian Massif. Mineral Soc Pol Spec Pap 37:32–36

Jeambrun M, Giot D, Aubert M, Gachon A, Lenat JF, Belkessa R, d'Arcy D (1976) Notice explicative, Carte géol. France (1/50 000), feuille Thiers (694). Bureau Rech Géol Minières, Orléans, p 50

Kirstein LA, Davies GR, Heeremans M (2006) The petrogenesis of Carboniferous-Permian dyke and sill intrusions across northern Europe. Contrib Mineral Petrol 152:721–742

Krmíček L (2010) Pre-Mesozoic lampropjyres and lamproites of the Bohemian Massif (Czech Republic, Polanc, Germany, Austria). Mineral Soc Pol Spec Pap 37:37–46

Krmíček L, Halavínová M, Romer RL, Vašinová Galiová M, Vaculovič T (2014) Phlogopite/matrix, clinopyroxene/matrix and clinopyroxene/phlogopite trace-element partitioning in a calc-alkaline lamprophyre: new constraints from the Křižanovice minette. J Geosciences 59:87–96

Krmíček L, Romer RL, Timmerman MJ, Ulrych J, Glodny J, Přichystal A, Sudo M (2020a) Long-lasting (65 Ma) regionally contrasting late- to post-orogenic Variscan mantle-derived potassic magmatism in the Bohemian Massif. J Petrol 61(7)

Krmíček L, Romer RL, Cempírek J, Gadas P, Krmíčekova S, Glodny J (2020b) Petrographic and Sr-Nd-Pb-Li isotope characteristics of a complex lamproite intrusion from the Saxo-Thuringian Zone: A unique example of peralkaline mantle-derived melt differentiation. Lithos 374–375:105735

Kurze M, Seifert T, Weber H, Henjes-Kunst F (1998) Petrographie, Geochemie und Altersstellung der Lamprophyrgänge des Elbtalschierfergebirges (Sachsen). Zeitschrift Geol Wiss 26:193–202

Laurent O, Couzinié S, Zeh A, Vanderhaeghe O, Moyen JF, Villaros A, Gardieu V, Chelle-Michou C (2017) Protracted, coeval and mantle melting during Variscan late-orogenic evolution: U-Pb dating in the eastern French Massif Central. Int J Earth Sci 106:421–451

Le Gall J, Doré F, Gresselin F, Pareyn C (1989) Le magmatisme alcalin de la distension post-varisque dans le Nord du Massif armoricain: exemples des volcanites carbonifères du bassin de Carentan et des lamprophyres du Nord-Cotentin. Ann Soc Géol Du Nord 108:25–33

Le Maitre RW (2005, ed) Igneous rocks. A classification and glossary of terms. Recommendations of the International Union of Geological Sciences Subcommission on the Systematics of Igneous Rocks. Cambridge University Press, 2nd edn, p 236

Leroy J, Sonnet J (1976) Contribution à l'étude géochimique des filons de lamprophyres recoupant le granite à deux micas de Saint-Sylvestre (Massif central français). CR Acad Sci Paris 283 sér D:1477–1480

Leutwein F, Chauris L, Sonet J, Zimmerman JL (1969) Etudes géochronologiques et géotectoniques dans le Nord-Finistère (Massif armoricain). Sciences De La Terre, Nancy 14(4):329–359

Leutwein F, Sonet J, Zimmerman JL (1972) Dykes basiques du Massif armoricain septentrional. Contribution à leur étude géochronologique. CR Acad Sci Paris 275 sér D:1327–1330

McDonough WC, Sun SS (1995) The composition of the Earth. Chem Geol 120:223–253

Mikulski SZ, Williams IS (2010a) SHRIMP zircon study of a spessartite dyke from the Klodzko-Zloty Stok granite, Chwallslaw (Sudetes). Mineral Soc Pol, Spec Pap 37:49

Mikulski SZ, Williams IS (2010b) Lamprophyres from the Żeleźniak igneous rock suites (Kaczawa Mountains) – geochemistry, petrography and preliminary SHRIMP zircon ages. Mineral Soc Pol Spec Pap 37:50–51

Molina JF, Moreno JA, Castro A, Rodriguez C, Fershtater GB (2015) Calcic amphibole thermobarometry in metamorphic and igneous rocks: new calibrations based on plagioclase/amphibole Al-Si partitioning and amphibole-liquid Mg partitioning. Lithos 232:286–305

Molina JF, Cambeses A, Moreno JA, Morales I, Lázaro C, Montero P, Bea F (2021) A cautionary note on amphibole geobarometry. Environ Sci Proc 6:17

Monjoie P, Bussy F, Schaltegger U, Mulch A, Lapierre H, Pfeifer H-R (2007) Contrasting magma types and timing of intrusion in the Permian layered mafic complex of Mont Collon (Western Alps, Valais, Switzerland): evidence from U/Pb zircon and $^{40}Ar/^{39}Ar$ amphibole dating. Swiss J Geosci 100:125–135

Neubauer F, Dallmeyer RD, Fritz H (2003) Chronological constraints of late- and post-orogenic emplacement of lamprophyre dykes in the southeastern Bohemian Massif, Austria. Schweiz Mineral Petrogr Mitt 83:317–330

Orejana D, Villaseca C, Billström K, Paterson BA (2008) Petrogenesis of Permian alkaline lamprophyres and diabases from the Spanish Central System and their geodynamic context within western Europe. Contrib Mineral Petrol 156:477–500

Pearce JA (2008) Geochemical fingerprinting of oceanic basalts with applications to ophiolite classification and the search for Archaean oceanic crust. Lithos 100:14–48

Pouchou JL, Pichoir F (1991) Quantitative analysis of homogeneous or stratified microvolumes applying the model "PAP." In: Heinriche DE (ed) Electron Probe Quantitation. Plenum Press, New York, pp 31–75

Pouclet A (2016) Sortie géologique de Vairé – Brétignolles - Crois-de-Vie. Association Vendéenne de Géologie, avg85.fr. Bull 16:10–36

Pouclet A, Alvaro JJ, Bardintzeff JM, Gil Imaz A, Monceret E, Vizcaïno D (2017) Cambrian-early Ordovician volcanism across the South Armorican and Occitan domains of the Variscan Belt in France: Continental break-up and rifting of the northern Gondwana margin. Geosci Front 8:25–64

Putirka K (2016) Amphibole thermometers and barometers for igneous systems and some implications for eruption mechanisms of felsic magmas at arc volcanoes. Am Min 101:841–858

Ridolfi F, Renzulli A, Puerini M (2010) Stability and chemical equilibrium of amphibole in calc-alkaline magmas: an overview, new thermobarometric formulations and application to subduction-related volcanoes. Contrib Mineral Petrol 160:45–66

Ridolfi F, Renzulli A (2012) Calcic amphiboles in calc-alkaline and alkaline magmas: thermobarometric and chemometric empirical equations valid up to 1,130°C and 2.2 GPa. Contrib Mineral Petrol 167:877–895

Rieder M, Cavazzini G, D'yakonov YS, Frank-Kamenetskii VA, Gottardi G, Guggenheim S, Koval PV, Müller G, Neiva AMR, Radoslovich EW, Robert J-L, Sassi FP, Takeda H, Weiss Z, Wones DR (1998) Nomenclature of the micas. Can Mineral 36:41–48

Journal : Large 710 | Article No : 786 | Pages : 25 | MS Code : 786 | Dispatch : 1-7-2022

Righter K, Carmichael ISE (1996) Phase equilibria of phlogopite lamprophyres from western Mexico: biotite-liquid equilibria and *P-T* estimates from biotite-bearing igneous rocks. Contrib Mineral Petrol 123:1–21

Roach A, Rutherford M (2003) Phlogopite thermometer calibration and use: magmatic history and processes in the Roman Potassic Province. Am Geophys Union Fall Meeting 2003, abstract #V41C-0313

Rock NMS (1987) The nature and origin of lamprophyres: an overview. In Fitton JG, Upton BGJ (eds) Alkaline igneous rocks. Geol Soc London Spec Pub 30:191–226

Rock NMS (1991) Lamprophyre. Blackie and Son Ltd., Glasgow and London, p 285

Scarrow JH, Bea F, Montero P, Molina JF, Vaughan APM (2006) A precise late Permian $^{40}Ar/^{39}Ar$ age for the central Iberian camptonitic lamprophyres. Geol Acta 4:451–459

Scarrow JH, Molina JF, Bea F, Montero P, Vaughan APM (2011) Lamprophyre dikes as tectonic markers of the late orogenic transtension timing and kinematics: A case study from the Central Iberian Zone. Tectonics 30:TC4007

Schaltegger U, Schneider JL, Maurin JC, Corfu F (1996) Precise U-Pb chronometry of 345–340 Ma old magmatism related to syn-convergence extension in the Southern Vosges (Central Variscan Belt). Earth Planet Sci Lett 144:403–419

Seifert T (2008) Metallogeny and petrogenesis of lamprophyres in the Mid-European Variscides. Technische Universität Bergakademie Freiberg, Germany, IOS Press BV publisher, Amsterdam

Soder C (2017) Geochemistry and petrology of lamprophyres from the Hellenides and the European Variscides. PhD thesis, Univ Heidelberg, p185

Soder CG, Romer RL (2018) Post-collisional potassic-ultrapotassic magmatism of the Variscan orogen: implications for mantle metasomatism during continental subduction. J Petrol 59:1007–1034

Steiger RW, Jäger E (1977) Subcommission of geochronology: convention on the use of decay constants in geo- and cosmochronology. Earth Planet Sci Lett 36:359–362

Štemprok M, Dolejš D, Holub FV (2014) Late Variscan calc-alkaline lamprophyres in the Krupka ore district, Eastern Krušné hory/Erzgebirge: their relationship to Sn-W mineralization. J Geosciences 59:41–68

Sun SS, McDonough WH (1989) Chemical and isotopic systematic of oceanic basalts: implications for mantle composition and processes. In: Saunders AD, Norry MJ (eds) Magmatism in the ocean basins, Geol Soc London Spec Pub 42:313–345

Tabaud AS, Janoušek V, Skrzypek E, Schulmann K, Rossi P, Whitechurch H, Guerrot C, Paquette JL (2015) Chronology, petrogenesis and heat sources for successive Carboniferous magmatic events in the Southern-Central Variscan Vosges Mts (NE France). J Geol Soc London 172:87–102

Thorpe RS, Cosgrove ME, Van Calsteren PWC (1986) Rare earth element, Sr- and Nd-isotope evidence for petrogenesis of Permian basaltic and K-rich volcanic rocks from south-west England. Min Mag 50:481–490

Turillot P, Augier R, Monié P, Faure M (2011) Late orogenic exhumation of the Variscan high-grade units (South Armorican Domain, western France), combined structural and 40Ar/39Ar constraints. Tectonics 30:TC5007

Turpin L, Velde D, Pinte G (1988) Geochemical comparison between minettes and kersantites from the Western European Hercynian orogen: trace element and Pb-Sr-Nd isotope constraints on their origin. Earth Planet Sci Lett 87:73–86

Velde D (1969) Les micas des lamprophyres : kersantites, minettes et lamproïtes. Bull Soc Fr Minéral Cristallogr 92:203–223

Velde D (1971) Les kersantites : études des lamprophyres à plagioclase et biotite. Bull Soc Fr Minéral Cristallogr 94:411–426

von Seckendorff V, Timmerman MJ, Kramer W, Wrobel P (2004) New $^{40}Ar/^{39}Ar$ ages and geochemistry of late Carboniferous-early Permian lamprophyres and related volcanic rocks in the Saxothuringian Zone of the Variscan Orogen (Germany). In: Wilson M, Neumann ER, Davies GR, Timmerman MJ, Heermans M, Larsen BT (eds) Permo-Carboniferous magmatism and rifting in Europe. Geol Soc London Spec Pub 223:335–359

Wagner C, Velde D, Joron JL (1992) Intrusions tardives dans le socle du forage scientifique de Sancerre-Couy. Géol Fr 3–4:147–150

Werner O, Lippolt HJ (1998) Datierung von postkinematischen Intrusionsphasen des Erzgebirges: Thermische und hydrothermale Überprägung der Nebengesteine. Terra Nova 98(2):100–103

Woodhead JD, Hergt JM, Davidson JP, Eggins SM (2001) Hafnium isotope evidence for 'conservative' element mobility during subduction processes. Earth Planet Sci Lett 192:331–346

Zang W, Fyfe WS (1995) Chloritization of the hydrothermally altered bedrock at the Igarapé Bahia gold deposit, Carajas, Brazil. Min Deposita 30:30–38

Zeitlhofer H, Grasemann B, Petrakakis K (2016) Variscan potassic dyke magmatism of durbachitic affinity at the southern end of the Bohemian Massif (Lower Austria). Int J Earth Sci 105:1175–1197

Publisher's Note Springer Nature remains neutral with regard to jurisdictional claims in published maps and institutional affiliations.

Journal : **Large 710**	Article No : **786**	Pages : **25**	MS Code : **786**	Dispatch : **1-7-2022**

Journal:	**710**
Article:	**786**

Author Query Form

Please ensure you fill out your response to the queries raised below and return this form along with your corrections

Dear Author

During the process of typesetting your article, the following queries have arisen. Please check your typeset proof carefully against the queries listed below and mark the necessary changes either directly on the proof/online grid or in the 'Author's response' area provided below

Query	Details Required	Author's Response
AQ1	Please check and confirm that the authors and their respective affiliations have been correctly identified and amend if necessary.	
AQ2	Soder (2008); Rudnick and Gao (2004); Skrzypek et al. 2012 and Tabaud et al. 2014 were mentioned in the manuscript; however, this were not included in the reference list. As a rule, all mentioned references should be present in the reference list. Please provide the reference details to be inserted in the reference list.	
AQ3	References Mikulski and Williams (2010) and Tabaud et al. (2015) were provided in the reference list; however, these were not mentioned or cited in the manuscript. As a rule, if a citation is present in the text, then it should be present in the list. Please provide the location of where to insert the reference citation in the main body text. Kindly ensure that all references are cited in ascending order.	